

Glycosaminoglycan-mimetic infernan grafted with poly(N-isopropylacrylamide): Toward a thermosensitive polysaccharide

Fillaudeau Arnaud ¹, Cuenot Stéphane ^{2,*}, Makshakova Olga ³, Traboni Serena ⁴, Sinquin Corinne ¹, Hennetier Marie ⁵, Bedini Emiliano ⁴, Perez Serge ⁶, Collicec Jouault Sylvia ¹, Zykwinska Agata ^{1,*}

¹ Ifremer, MASAE Microbiologie Aliment Santé Environnement, F-44000 Nantes, France

² Nantes Université, CNRS, Institut des Matériaux Jean Rouxel, IMN, Nantes, France

³ Kazan Institute of Biochemistry and Biophysics, FRC Kazan Scientific Center of RAS, Lobachevsky Str., 2/31, 420111 Kazan, Russian Federation

⁴ Department of Chemical Sciences, University of Naples Federico II, Complesso Universitario Monte S. Angelo, via Cintia 4, I-80126 Napoli, Italy

⁵ Plateforme Toulouse Field-Flow Fractionation Center, TFFFC, Ecole d'Ingénieurs de Purpan, Toulouse, France

⁶ Centre de Recherches sur les Macromolécules Végétales, Université de Grenoble Alpes, Centre National de la Recherche Scientifique, Grenoble, France

* Corresponding authors : Stéphane Cuenot, email address : Stephane.Cuenot@cnrns-imn.fr ; Agata Zykwinska, email address : Agata.Zykwinska@ifremer.fr

Abstract :

Glycosaminoglycans (GAGs) are essential constituents of the cell surface and extracellular matrix, where they are involved in several cellular processes through their interactions with various proteins. For successful tissue regeneration, developing an appropriate matrix supporting biological activities of cells in a similar manner than GAGs remains still challenging. In this context, this study aims to design a thermosensitive polysaccharide that could further be used as hydrogel for tissue engineering applications. For this purpose, infernan, a marine bacterial exopolysaccharide (EPS) endowed with GAG-mimetic properties was grafted with a thermosensitive polymer, poly(N-isopropylacrylamide) (pNIPAM). Eight grafted polysaccharides were obtained by varying EPS/pNIPAM molar ratio and the molecular weight of pNIPAM. Their physicochemical characteristics and their thermosensitive properties were determined using a multi-technique, experimental approach. In parallel, molecular dynamics and Monte Carlo simulations were applied at two different scales to elucidate, respectively, the molecular conformation of grafted infernan chain and their ability to form an infinite network undergoing a sol-gel transition near the percolation, a necessary condition in hydrogel formation. It comes out from this study that thermosensitive infernan was successfully developed and its potential use in tissue regeneration as a hydrogel scaffold will further be assessed.

Keywords : exopolysaccharide, pNIPAM, molecular dynamics, AFM, NMR, Monte Carlo simulations

1. Introduction

Glycosaminoglycans (GAGs), linear anionic heteropolysaccharides are critical constituents of both the cell surface and extracellular matrix (ECM) of animal tissues. Presenting a high charge density, GAGs regulate several cellular behaviors (adhesion, migration, proliferation, differentiation) through interactions with multiple proteins (e.g. growth factors, cytokines) (Gandhi & Mancera, 2008; Perez *et al.*, 2023). GAGs are therefore essential elements of the cellular microenvironment responsible for the development and maintenance of physiological functions, inspiring in this way a large number of tissue engineering strategies in the search for bio-mimetic scaffolds (Baei, Daemi, Aramesh, Baharvand, & Eslaminejad, 2023; Celikkin *et al.*, 2017; Menezes, Vincent, Osorno, Hu, & Arinzeh, 2023). Although their exploitation was initially based on extraction from animal organisms (bovine, porcine, chicken,

shark), the difficulties of standardization and contamination of batches encountered in recent years led to the development of alternative sources of GAGs (Badri, Williams, Linhardt, & Koffas, 2018). The biosynthesis of these bioactive polysaccharides by microorganisms, such as bacteria constitutes an interesting approach, offering a controlled production in bioreactors, thus allowing to obtain batches of constant quality with high purity in a short time and with a high potential yield (Cimini, Bedini, & Schiraldi, 2023; Kang *et al.*, 2018; Liu, Guo, Chen, Liu, & Gao, 2023). Bacteria from deep-sea hydrothermal vents exhibit an atypical chemodiversity, reflecting the environment in which they evolve (Delbarré-Ladrat, Siquin, Lebellenger, Zykwinska, & Collic-Jouault, 2014; Zykwinska *et al.*, 2019a). This is particularly the case of the marine Gram-negative bacterium *Alteromonas infernus*, secreting an original highly branched exopolysaccharide (EPS) called infernan. G 1785 EPS) (Raguénès *et al.*, 1997; Roger, Kervarec, Ratiskol, Collic-Jouault, & Chevlot, 2004). In our previous studies, the GAG-mimetic properties of infernan, resulting from the presence of both sulfate groups and uronic acid (UA) residues, were demonstrated *in vitro* and *in vivo* (Rederstorff *et al.*, 2011, 2017). Indeed, the addition of native EPS of HMW ($\sim 10^6$ g/mol) into silated hydroxypropyl methylcellulose (Si-HPMC) hydrogel supported the viability and proliferation of chondrocytes and osteoblasts cultured in two and three dimensions (Rederstorff *et al.*, 2011). *In vivo*, this infernan-enriched hydrogel implanted in the subcutis of nude mice allowed the synthesis of a cartilage-like extracellular matrix, rich in sulfated GAGs and type II collagen, by incorporated chondrocytes (Rederstorff *et al.*, 2017). Indeed, due to its natural affinity towards the growth factors, such as TGF- β 1 and BMP-2, native infernan can be exploited in tissue regeneration (Rederstorff *et al.*, 2017). The presence of this HMW polysaccharide also improved the mechanical properties of the final hydrogel (Rederstorff *et al.*, 2011, 2017). Thus, possessing the

functional properties (biological and structural) of GAGs, using infernan as a scaffold to support cellular activities, including cell adhesion and proliferation seems promising. While medium-molecular weight infernan derivatives display gelling properties with calcium and can be structured in microgels delivering growth factors for tissue engineering purposes (Gélébart *et al.*, 2022; Zykwinska *et al.*, 2019b, 2022), too high chain length of the native EPS limits its ionic gelation through properly establishing junction zones mediated by calcium ions (Makshakova, Zykwinska, Cuenot, Collic-Jouault, & Perez, 2022). Therefore, modification of native infernan is necessary in order to provide gelling properties to the polysaccharide for its further use as hydrogel in tissue engineering. Among the simple modification that can be envisaged, the grafting of smart polymers sensitive to a stimulus, particularly the temperature, seems ideal for biomedical applications (Ruel-Gariépy & Leroux, 2007). As such, due to its rapid coil-to-globule phase transition at lower critical solution temperature (LCST $\sim 32^{\circ}\text{C}$) below physiological temperature, poly(*N*-isopropylacrylamide) (pNIPAM) is one of the most widely studied thermosensitive polymer with a huge potential in tissue engineering (Rana & De la Hoz Siegler, 2021). Its temperature-dependent properties arise from the rearrangement of water molecules near hydrophilic and hydrophobic groups of pNIPAM above LCST, leading to reduction of the exposed hydrophobic surface by their clustering (Ortiz de Solorzano, Bejagam, An, Singh, & Deshmukh, 2020; Tavagnacco, Zaccarelli, & Chiessi, 2018). PNIPAM with various terminal groups ($-\text{NH}_2$, $-\text{COOH}$, $-\text{N}_3$) and molecular weights can be tailored for grafting on multiple polymers. Several polysaccharides were thus grafted with pNIPAM, amongst alginate (Ciocoiu, Staikos, & Vasile, 2018), hyaluronan (Atoufi *et al.*, 2019; D'Este *et al.*, 2016) and chitosan (Ding *et al.*, 2020), allowing the development of custom grafted polymers that can be exploited in tissue engineering.

In this context, the objective of the present study was to obtain a thermosensitive polysaccharide by grafting GAG-mimetic infernan with pNIPAM and to characterize the physicochemical characteristics, *i.e.* degree of grafting, molecular weight, conformation and morphology of grafted polysaccharide chains and their phase transition properties. For this purpose, different grafted polymers were synthesized using amino-terminated pNIPAM and 1-ethyl-3-(3-dimethylaminopropyl)carbodiimide hydrochloride/*N*-hydroxysuccinimide (EDC/NHS) coupling chemistry by varying EPS to pNIPAM molar ratios and molecular weights of pNIPAM. The impact of these parameters on molecular characteristics of grafted polymers and their thermosensitive properties was then evaluated using a complementary approach involving several experimental techniques, amongst Friction Inlet-Asymmetrical Flow Field-Flow Fractionation coupled with Multi-Angle Light Scattering and Refractive Index detectors (FI-AF4-MALLS-dRI), Dynamic Light Scattering (DLS), Attenuated Total Reflection - Fourier Transform Infrared (ATR-FTIR) spectroscopy, Nuclear Magnetic Resonance (NMR) and Atomic Force Microscopy (AFM). In parallel, a theoretical approach exploring molecular dynamics (MD) simulations was applied to establish the molecular conformations of infernan grafted with pNIPAM chains at different levels, thus allowing a better understanding of intra and inter-chain interactions occurring in solution. Complementary Monte Carlo simulations were also performed to investigate the ability of grafted polysaccharide chains to form an infinite network by only assuming attractive inter-chain interactions between pNIPAM grafts. The main hypothesis of the present study was to assess if the degree of grafting tuned by EPS/pNIPAM molar ratio and pNIPAM molecular weight impacts the physicochemical and thermosensitive properties of grafted polysaccharides. The knowledge of these parameters remains essential for the future use of EPS-pNIPAM polymers as hydrogels for tissue engineering purposes.

2. Materials and Methods

2.1. Production of the native infernan by *A. infernus* fermentation and its characterization

Infernan was produced by fermentation of *A. infernus* as described earlier (Raguénès *et al.*, 1997). Briefly, bacteria were cultured at 25°C, pH 7.4 in a 30 L bioreactor (Techfors, INFORS, Switzerland) in Zobell medium composed of 33.3 g/L of aquarium salts, 5 g/L of tryptone and 1 g/L of yeast extract. *A. infernus* uses glucose for EPS synthesis, added at 30 g/L at the beginning of the batch. After 48h, EPS recovered in the supernatant after centrifugation (9000 g, 45 min) was purified by sequential filtration and final ultrafiltration steps, (MWCO 100,000 g/mol) before being freeze-dried. Native EPS was characterized by its monosaccharide composition and sulfur content, as previously described (Gélébart *et al.*, 2022).

2.2. Grafting of pNIPAM-NH₂ on infernan by carbodiimide chemistry

EPS-pNIPAM polymers were prepared by grafting the amino-terminated (-NH₂) commercial pNIPAM-NH₂ to the carboxyl (-COOH) functions of uronic acids (UA) of native EPS, through carbodiimide chemistry, using EDC/NHS as coupling agents. Two molecular weights of pNIPAM-NH₂ were used either pNIPAM of Mn 5,500 g/mol (p5) (Sigma, Aldrich) or pNIPAM of Mn 20,000 g/mol (p20) (Polymer Source, Canada). Various molar ratios COOH(EPS):NH₂(pNIPAM) were applied : 0.65, 1.0, 2.1, 3.5 and 1.3, 2.3, 3.8, 6.3 for EPS/p5 and EPS/p20 coupling reactions, respectively (Table 1), in order to obtain four different EPS-pNIPAM polymers by pNIPAM molecular weight. In addition, the condition with the highest molar ratio EPS:pNIPAM (condition 4) was carried out by mixing EPS and pNIPAM without EDC/NHS adding to generate the conditions 4* and 8*, corresponding to ungrafted EPS-p5-0% and EPS-p20-0%. For infernan grafting, EPS and pNIPAM-NH₂ were separately dissolved in 1

mL of MES buffer (50 mM, pH 4.8) at room temperature. After 24h, both solutions were mixed, and EDC/NHS were added (except conditions 4* and 8*). The reaction mixture was stirred at 250 rpm for 6h at 20°C before a new EDC/NHS addition to potentialize the pNIPAM-NH₂ graft. The final EDC/NHS molar ratio COOH:EDC:NHS was 1:1.6:1.6. After overnight incubation, the products were dialyzed (MWCO 50,000 g/mol) against 0.3 M NaCl (24 h) and Milli-Q water (48 h) to remove both coupling agent and ungrafted pNIPAM, and freeze-dried. EPS-pNIPAM grafting was performed in triplicate.

Table 1. Reaction conditions of pNIPAM-NH₂ (-NH₂) grafting on EPS (-COOH) by carbodiimide chemistry (EDC/NHS) for a final molar ratio COOH/EDC/NHS = 1:1.6:1.6 (except conditions 4* and 8*).

Reaction condition	Polym er design ation (a)	EPS (mg)	COOH of EPS (10 ⁻⁵ mol) (b)	pNIPAM-NH ₂ (mg)	NH ₂ of pNIPAM-NH ₂ (10 ⁻⁵ mol)	Molar ratio COOH/NH ₂
1	EPS-p5-16%	10	1.9	161	2.9	0.65
2	EPS-p5-8%	20	3.8	200	3.6	1.0
3	EPS-p5-3%	40	7.6	200	3.6	2.1

4	EPS- p5-2%	40	7.6	120	2.2	3.5
4*	EPS- p5-0%	40	7.6	120	2.2	3.5
5	EPS- p20- 6%	5	0.95	151	0.76	1.3
6	EPS- p20- 3%	10	1.9	161	0.81	2.3
7	EPS- p20- 1%	20	3.8	200	1.0	3.8
8	EPS- p20- 0.2%	20	3.8	120	0.60	6.3
8*	EPS- p20- 0%	20	3.8	120	0.60	6.3

(a) Polymer designation “EPS-pX-Y%” includes EPS, pNIPAM of either Mn 5,500 g/mol (p5) or Mn 20,000 g/mol (p20) (X) as well as the degree of UA grafting (Y), calculated from the data shown in Table 2.

Conditions 4* and 8* were carried out by mixing EPS and pNIPAM without EDC/NHS adding.

$$(b) \text{ COOH of EPS (mol)} = \frac{Mn \text{ EPS}}{M \text{ repeating unit}} \times 3 \text{ UA in repeating unit} \times \text{mol EPS}$$

Mn p5, 5,500 g/mol; Mn p20, 20 000 g/mol; Mn EPS, 900 000 g/mol; M repeating unit of EPS, 1587 g/mol with 3 UA residues (sodium salt).

2.3. Molecular characterization of EPS-pNIPAM grafted polymers

2.3.1. Molecular dynamics (MD) simulations

The initial geometry of infernan was constructed according to the sequence described in Fig. 1 (showing the chemical structure of infernan) and using equilibrated torsion angles reported in Makshakova *et al.* (2022). The length of the infernan fragment used in MD simulations was limited by four repetitive backbone blocks (or repeating units) and three side chains. The analysis aims to investigate the influence of short-range interactions of pNIPAM covalently attached to the UA on infernan. Three molecular systems were constructed: 1) linear backbone of infernan grafted at galacturonic acid 2-O sulfated (GalA2S) by three pNIPAM chains, 2) branched infernan partially grafted at glucuronic acid (GlcA) in the side chain (with three pNIPAM chains per nine carboxylate groups) and 3) branched infernan fully grafted at three UA residues per repeating unit (with nine pNIPAM chains per nine carboxylate groups). For this purpose, one infernan fragment was placed into a water box with periodic boundary conditions. Sodium ions were added to neutralize the charge of the molecular system (see precise composition for each system in Table S1). The simulations were carried out using the AMBER18 program package (Case *et al.*, 2018) in the isotherm isobar thermodynamic ensemble. GLYCAM06j force-field parameters (Kirschner *et al.*, 2008) were used for the polysaccharide and GAFF parameters for pNIPAM moiety (Wang, Wolf, Caldwell, Kollman & Case, 2004; Wang, Wang, Kollman & Case, 2006) (more details in Supporting Information

Figure S1, Table S2). The AMBER force field and the TIP3P model for water molecules were used for ions. A time step of 2 fs was applied with the SHAKE algorithm (Ryckaert, Ciccotti, & Berendsen, 1997) constrained bonds involving hydrogen atoms. Particle Mesh Ewald (PME) (Essmann *et al.*, 1995) handled long-range electrostatic interactions. An 8 Å cut-off value for electrostatic interactions was used in simulations; a rectangular water box was selected, having dimensions commensurate to the size of the molecule under investigation. The temperature and the pressure were kept constant using a Langevin thermostat with a collision frequency of 2 ps^{-1} and a weak coupling anisotropic algorithm with a relaxation time of 2 ps respectively. Initial velocities were derived from a Maxwellian distribution at 100 K using a random seed for each simulation. Short equilibration phases were performed in the NVT and NPT ensemble. Finally, the production phases were performed on totally "relaxed" systems in the NPT ensemble at 300 K with trajectories in the range of 400 ns. VMD was used for the graphical representation (Humphrey, Dalke, & Schulten, 1996).

2.3.2. Frit Inlet-Asymmetrical Flow Field-Flow Fractionation coupled with Multi-Angle Light Scattering and Refractive Index detectors (FI-AF4-MALLS-dRI)

FI-AF4-MALLS-dRI was applied to characterize the degree of infernan grafting with pNIPAM, the molecular weight of grafted polysaccharides and their conformation in solution after separation according to the polymer size. The AF4 instrument was an Eclipse AF4 separation system (Wyatt Technology Europe, Germany) coupled with 8 angle Dawn Heleos II 8+ multi-angle light scattering detector (Wyatt Technology, USA) operated at a wavelength of 662 nm, calibrated with toluene and normalized with the inter-detector delays and band broadening calculations with bovine serum albumin (Mw 66,400 g/mol) and an Optilab T-Rex

differential refractive index detector (Wyatt Technology, USA) operated at a wavelength of 658 nm. AF4 analyses were done using a Thermo Scientific Dionex UltiMate3000 HPLC System with pump and thermostated autosampler set at 20°C. A channel composed of regenerated cellulose membrane (MWCO 5,000 g/mol) with a 350 µm spacer was used. All grafted EPS were prepared by keeping the polysaccharide concentration in all the samples constant at 1 mg/mL. Injections (50 µL at 0.2 mL/min) were performed in triplicate for each sample separated by blank for a correction baseline. The detector flow rate was kept constant at 1 mL/min. At the beginning of elution (in 0.1 M ammonium acetate), the cross flow was maintained at 2 mL/min for 2 min. It was then decreased exponentially from 2 mL/min to 0.04 mL/min in 18 min. The cross-flow was kept constant at 0.04 mL/min for an additional 20 min and reduced at 0 mL/min for 2 min. The collected data were analyzed using Astra 7.1.2. software with a Zimm fit for pNIPAM samples (p5 and p20) and Berry second-order polynomial fit for EPS and grafted EPS samples. The dn/dc refractive index increment was measured for EPS (0.1267 ± 0.001 , $n=5$), p5 (0.1717 ± 0.0001 , $n=2$) and p20 (0.1703 ± 0.0001 , $n=2$) for n dilution range between 0.1 and 1 mg/mL in 0.1 M ammonium acetate. The average dn/dc value of 0.1740 was then used for pNIPAM samples. The dn/dc of EPS was also used for grafted EPS.

2.3.3. Attenuated Total Reflection - Fourier Transform Infrared (ATR-FTIR) spectroscopy

ATR-FTIR spectra of EPS, pNIPAM (p5 and p20) and EPS-pNIPAM polymers were recorded using a VERTEX 70 FTIR spectrometer (Bruker) in ATR mode using a diamond crystal. Spectra were recorded in the range $4000\text{--}500\text{ cm}^{-1}$ at a resolution of 4 cm^{-1} with 100 scans per spectrum using OPUS software.

2.3.4. Nuclear magnetic resonance (NMR)

1D- ^1H - and DOSY) and 2D-NMR (COSY and DEPT-HSQC) spectra were measured for

EPS, pNIPAM (p5) and EPS-pNIPAM (EPS-p5-2% and EPS-p5-0%) samples using a Bruker Avance-III (^1H : 600 MHz, ^{13}C : 150 MHz) instrument equipped with a cryo-probe in D_2O (acetone as the internal standard, ^1H : $(\text{CH}_3)_2\text{CO}$ at δ 2.22 ppm; ^{13}C : $(\text{CH}_3)_2\text{CO}$ at δ 31.5 ppm) at 40°C . The data were processed using the data analysis packages integrated with Bruker TopSpin 4.0.5 software. Gradient-selected COSY experiments were performed using spectral widths of 5000 Hz in both dimensions, and data sets of 2048×256 points. $^1\text{H},^{13}\text{C}$ -DEPT-HSQC experiments were measured in the ^1H -detected mode via single quantum coherence with proton decoupling in the ^{13}C domain, using data sets of 2048×256 points and typically 100 increments. ^1H -DOSY experiments were measured with a diffusion time of 100 ms.

2.4. Determination of thermosensitive properties of EPS-pNIPAM grafted polymers

2.4.1. UV-visible spectroscopy

The thermosensitive properties of EPS-pNIPAM polymers were evaluated using UV-visible spectroscopy (Varioskan LUX, ThermoFisher). The thermal phase transition in samples at 1 mg/mL in PBS (pH 7.4) was monitored by measuring the absorbance at 550 nm from 25°C to 38°C with 10 minutes of thermal equilibrium for each temperature.

2.4.2. Dynamic Light Scattering (DLS)

The thermo-responsive behavior of EPS, pNIPAM (p5 and p20) and EPS-pNIPAM polymers was studied by DLS. All samples were prepared at 1 mg/mL in PBS (pH 7.4) and used without pre-filtration to avoid modification of the polymer size. In addition, samples were prepared by setting the EPS concentration constant at 0.1 mg/mL. DLS measurements were carried out in triplicate on three independently synthesized samples using Zetasizer Pro (633 nm He-Ne laser, Malvern Instruments Ltd UK) equipped with a Peltier module at a fixed scattering angle of 173° at 25°C and 38°C with 10 minutes of thermal equilibrium for each temperature.

Data analysis was performed using Malvern Zetasizer Software 3.2.

2.4.3. Atomic force microscopy (AFM) imaging

Morphologies of grafted infernan chains were examined by AFM imaging. EPS, pNIPAM (p5 and p20) and EPS-pNIPAM polymers were prepared in water at 1 mg/mL. After 24h dissolution, solutions were incubated either at 25°C or 37°C for 30 min before being diluted at 5 µg/mL in water maintained at 25°C or 37°C. 10 µL of each solution were deposited onto freshly cleaved mica surface and dried at either 25°C or 37°C. The surface of samples was then imaged using NanoWizard® Atomic Force Microscope (JPK, Germany) operating in intermittent contact mode under ambient conditions. A standard rectangular cantilever (Nanosensors NCL-W) was used with a free resonance frequency of 165 kHz and a typical spring constant of 40 N/m. The radius curvature of the tip was ~5 nm. High-resolution images (10 µm x 10 µm and 2 µm x 2 µm) were recorded on at least three different zones of each sample. Image processing and height measurements were performed using JPK Data Processing software (JPK, Germany).

2.5. Investigation of inter-chain EPS-pNIPAM associations by Monte Carlo simulations

Monte Carlo simulations were used to model the ability of EPS-pNIPAM chains to form an infinite network. The hypothesis underlying these simulations is that the inter-chain interactions between pNIPAM drive the construction of the EPS-pNIPAM network. Considering the long calculation times, simulations were only carried out for EPS-p20 chains. In this case, ~5.9 % of UA of the EPS chain with a contour length of ~1 µm was used to graft pNIPAM chains with a contour length of ~30 nm. In all simulations, the space step was kept constant at 5 nm so an EPS-p20 chain was modelled by 200 pixels (contour length) with 12 grafted pNIPAM chains. For each EPS-p20 chain, the 12 positions of grafted chains along the EPS chain were randomly chosen. As the sol-gel transition of this system will occur above the LCST, where pNIPAM is in

its collapsed state, pNIPAM chains were modelled by refolded chains instead of freely chains. Simulations were performed on a two-dimensional square lattice of $L \times L$ sites with periodic boundary conditions imposed in both horizontal and vertical directions. From the initial state where all lattice sites were empty, the first chain was freely deposited with a random position on the lattice sites and a random conformation. Then, another chain with its random conformation was deposited randomly on empty sites. Its horizontal and vertical values defined a local rectangular box surrounding this conformation. One of the five random conformations generated inside this local box was randomly attempted to equilibrate the system, leading to a new trial configuration of the added chain. The energy difference, ΔH , between the trial and the old configurations was calculated to determine if the conformation change was accepted by using the standard Metropolis acceptance criterion (Wu, Sarntinoranont, & Zia, 2008; Zykwinska, Pihet, Radji, Bouchara, & Cuenot, 2014). If ΔH was negative (*i.e.* the energy of the system was minimized), the trial configuration was accepted and the procedure was repeated by choosing another chain. If ΔH was positive the conformation change was accepted or rejected according to the standard Metropolis acceptance criterion probability. The system energy was calculated for a given configuration by only considering short-range attractive inter-chain interactions between pNIPAM. In this way, the shortest distances between the 12 pNIPAM chains of the trial conformation and the pNIPAM chains belonging to the neighbouring EPS-p20 chains were considered (more details in Supporting Information).

The analysis of simulations consisted in evaluating the formation of clusters, which correspond to an island of connected neighbouring chains. When the occupation probability ϕ (*i.e.* polymer concentration) defined by the ratio of the number of lattice sites occupied by EPS-p20 chains to the total number of sites increases, the size of clusters increases and neighboring clusters can

progressively merge. The limit case, called percolation, was reached when at least one cluster formed a continuous path by connected chains from one side of the square lattice to the opposite one. The percolation threshold ϕ_c (*i.e.* critical concentration) for a finite size L of the lattice was defined as the occupation probability at the percolation. To evaluate ϕ_c from simulations, the minimum and maximum coordinates of each cluster were determined in function of ϕ (*i.e.* for each new EPS-p20 chain added on the lattice). The percolation threshold occurred when the difference between these coordinates for the same cluster (in one direction) exceeded L . To study the influence of the lattice size on ϕ_c , simulations were carried out for different values of L (1 μm , 2 μm , 5 μm and 10 μm). Larger lattices were not simulated due to the too-long calculation times. At least 50 independent simulations were systematically performed for each set of parameters (L , ϕ) for statistical analysis of simulations. The percolation probability was calculated from these simulations as the ratio of the number of percolated networks to the number of generated networks.

3. Results and discussion

Native infernan produced by *A. infernus* was first described by Roger *et al.* (2004) as a highly branched anionic heteropolysaccharide with a monosulfated nonasaccharide repeating unit (Fig. 1A). Recently, a novel disulfated octasaccharide repeating unit was proposed after mass spectrometry analysis performed on LMW infernan derivatives obtained after enzymatic depolymerization (Akoumany *et al.*, 2019). This finding was recently confirmed by 2D NMR analysis performed on LMW chemically depolymerized derivative (Colliec-Jouault *et al.*, 2023). In this new repeating unit, EPS backbone and side chain sequences are conserved; only the

terminal Glc of the side chain initially linked to Gal residue at C-6 was replaced by a sulfate group (Fig. 1A). The physicochemical composition, including monosaccharide composition, molar ratio and sulfur content of the native HMW infernan used in the present study, were presented in Table S3 (Supporting Information), in agreement with the previous studies (Gélébart *et al.*, 2022; Collic-Jouault *et al.*, 2023). The weight-average (M_w , 1.6×10^6 g/mol) and number-average (M_n , 0.9×10^6 g/mol) molecular weights, showed a slight dispersity of native infernan chains.

3.1. Molecular dynamics (MD) simulations of infernan grafted with pNIPAM chains

Since infernan contains three consecutive UA residues in its repeating unit (one galacturonic acid, GalA, in the backbone and two GlcA in the side chain), MD simulations were applied to assess the accessibility of the three UA for grafting with pNIPAM and to elucidate the molecular conformation of resulting grafted polysaccharide. The 3D structure of the octasaccharide repeating unit of infernan was built using torsion values related to the global energy minimum of each constituent disaccharide, as recently described (Makshakova *et al.*, 2022). The resulting structure presented in Fig. 1B, showing four repeating units with three side chains, remained somewhat extended with an end-to-end distance of 4.84 ± 0.28 nm (the per residue raise of 0.403 ± 0.023 nm). In the side chains, the branching of GlcA residues at 3-*O* and 2-*O* positions by α -glucosyl residues results in the formation of stable hydrogen bonds between the hydroxyl groups of glucosyl residues and the carboxylate groups of GlcA residues. Despite these interactions in the side chains, all three carboxylate groups (at GalA2S and two GlcA) in the repeating unit seem to be available for interaction and reaction with the pNIPAM terminal amino group. To study the effect of pNIPAM on the infernan extended conformation, pNIPAM chains were covalently bound to carboxylate groups of the polysaccharide. At the model extreme

substitution level, all carboxylate groups were grafted with pNIPAM chains (Fig. 1C). The degree of polymerization of pNIPAM was set to 21 to be comparable with the infernan fragment in length. During MD simulations at 300 K, pNIPAM chains come into contact inducing a bending of the infernan backbone, as indicated by a decrease of the end-to-end distance from ~5 nm to ~2 nm (Fig. 1C', Figure S2). To further investigate if the extended backbone would also collapse due to pNIPAM chains aggregation at a lower level of grafting, only one pNIPAM chain per repeating unit was linked to the side chain of infernan, corresponding to 33% of grafting (Fig. 1D). During the MD trajectory, the pNIPAM chains grouped and the end-to-end backbone distance decreased to 3 nm (Fig. 1D', Figure S2). The effect of the backbone bending was observed irrespectively of the place of grafting: either side chain (at GlcA) or backbone (at GalA2S) (Figure S2).

At a given density and length of the pNIPAM chains, their interactions in bunches stabilize their extended conformation. Such a behavior differs from that observed for an individual pNIPAM, where chain folding was observed, and from infernan with 100% grafting, where pNIPAM chains induce bending of the infernan to maximize their interactions. MD simulations showed the tendency of pNIPAM chains, when grafted to infernan, to interact with each other leading to the backbone bending. It implies that interactions between pNIPAM chains are more favorable than forces keeping the polysaccharide backbone linear; this effect occurs at a short-range level. The results from the investigation observed for short polysaccharide fragments can be extrapolated to a larger scale. In the regions enriched with pNIPAM grafting, the local extension of the polysaccharide backbone would exhibit a curvature shape due to pNIPAM chain interaction, resulting in the local infernan compaction. The backbone bending and its local compaction would make possible the interactions of pNIPAM chains from remote regions of

infernan, resulting in a global compaction of the macromolecular assembly (see the experimental proof in Section 3.3.3).

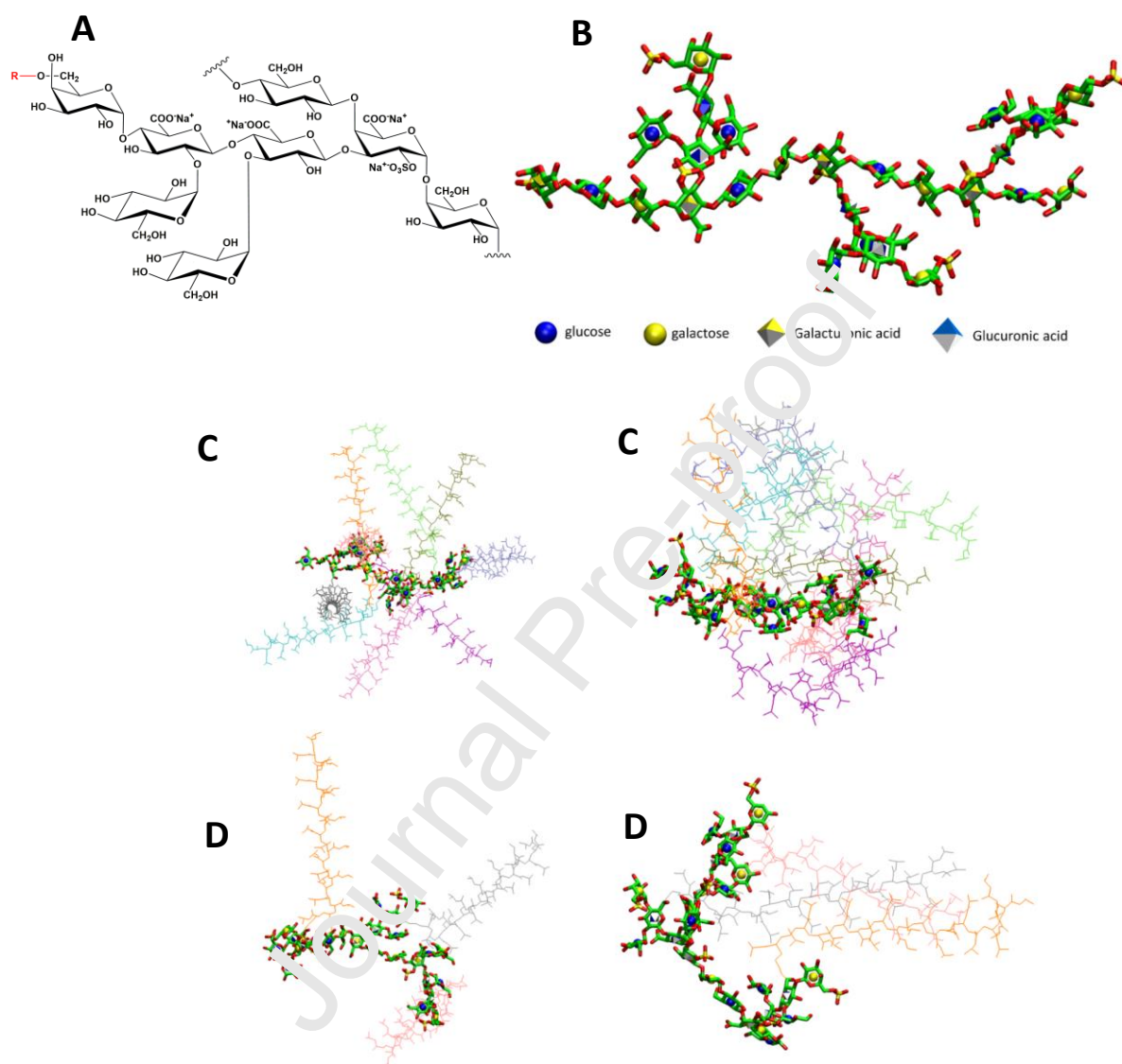


Fig. 1. MD simulations of three molecular systems: (A) The two types of infernan repeating unit: a monosulfated nonasaccharide repeating unit ($R = \beta\text{-Glc}$) (Roger *et al.*, 2004) and a disulfated octasaccharide repeating unit ($R = \text{SO}_3^- \text{Na}^+$) (Akoumany *et al.*, 2019; Collic-Jouault *et al.*, 2023), (B) four octasaccharide repeating units of infernan showing a linear backbone branched at GalA2S with three side chains, (C, C') branched infernan fully grafted at three UA residues per

building block, leading to nine pNIPAM chains per nine carboxylate groups and (D, D') branched infernan partially grafted at GlcA in the side chain with three pNIPAM chains per nine carboxylate groups. The representative structures are provided in Supporting Information.

3.2. Physico-chemical characterization of grafted EPS-pNIPAM polymers

3.2.1. Infernan grafting, molecular weight and conformation by FI-AF4-MALLS-dRI

Infernan was grafted with two amino-terminated pNIPAM-NH₂ of two molecular weights, either Mn 5,500 g/mol (p5) or Mn 20,000 g/mol (p20) at different COOH/NH₂ molar ratios (Table 1). The resulting grafted polysaccharides were characterized by FI-AF4-MALLS-dRI to determine their grafting density, molecular weight and conformation. If the standard fractionation technique using size exclusion chromatography (SEC) could be interesting for LMW macromolecules, adsorption and degradation by shear stress can occur for very HMW compounds as polysaccharides, especially if they are grafted with other polymers (Shin, Hwang, Cho, & Moon, 2007). An alternative method could be a fractionation of components offered by the AF4 technique, operating without a stationary phase. After focusing/relaxation steps, molecules are separated based on their translational diffusion coefficients by a longitudinal parabolic flow. Using a slit inlet system, without focus step, enables injection of higher amounts with better recovery than conventional FFF techniques and softer elution, thus preventing the aggregation of compounds on the membrane (Fuentes *et al.*, 2019; Lee, Kim, Choi, & Moon, 2017). FI-AF4 fractograms of EPS and p5 alone are presented in Fig. 2 (A, B). PNIPAM was mostly eluted from 1 to 9.5 min; its mass fraction was estimated at 96% for a recovery of 89% (pNIPAM domain). Most of the EPS was eluted from 9.5 to 18 min (73% of the mass fraction) (EPS domain). Fig. 2 C and D present FI-AF4 fractograms of four grafted EPS-p5 polymers and

ungrafted EPS-p5-0%, obtained by mixing EPS with pNIPAM without the addition of the coupling agent (EDC/NHS) (Table 1). Fractograms of EPS-p20 samples were presented in Fig. S3 (A, B). Two main peaks were always present, the first eluted in the pNIPAM domain, corresponding to free ungrafted pNIPAM remaining in the sample and the second in the EPS domain, matching with EPS or grafted EPS. It appeared that despite dialysis using 50,000 g/mol cut-off membrane, unreacted (free) pNIPAM was not completely removed and was still embedded in all samples, including the condition 4*, corresponding to ungrafted EPS (EPS-p5-0%).

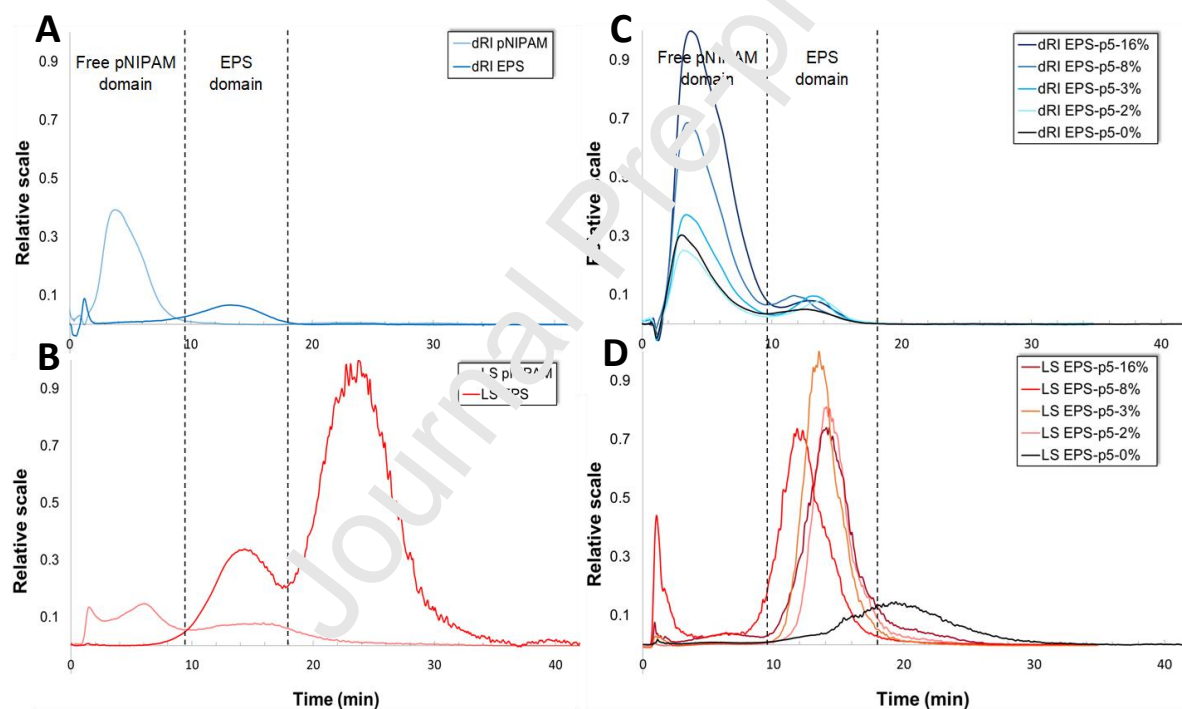


Fig. 2. FI-AF4 fractograms: (A) Differential refractive index (dRI) and (B) light scattering (LS) signals of EPS and pNIPAM 5,500 g/mol. (C) dRI and (D) LS signals of EPS-p5 samples.

The amount of grafted and free (ungrafted) pNIPAM was then estimated by taking into account:

(1) the known value of dn/dc refractive index increment of free pNIPAM, (2) the amount of

pNIPAM remaining in the sample after dialysis (and considering that only pNIPAM can be removed, keeping the amount of EPS unchanged), (3) the amount of injected pNIPAM for FI-AF4 analysis in EPS-pNIPAM samples (after subtraction of the EPS amount), (4) the amount of free pNIPAM quantified from FI-AF4-dRI (pNIPAM domain) and (5) by considering that this analysis allows the recovery of 89% of pNIPAM (Table 2). The FI-AF4-MALLS analysis allowed to distinguish between free ungrafted pNIPAM, still remaining in the sample despite the dialysis step, and pNIPAM efficiently grafted on the EPS backbone. Based on the amount of grafted pNIPAM, the efficiency of reaction, being the ratio between the weights of pNIPAM grafted and initially added, as well as the degree of grafting corresponding to the percentage of UA grafted on the infernan chain were determined (Table 2), using the following equations:

$$(a) \text{ Reaction efficiency (\%)} = \frac{\text{grafted pNIPAM (mg)}}{\text{initial pNIPAM (mg)}} \times 100 \%$$

$$(b) \text{ Number of UA grafted} = \frac{\text{grafted pNIPAM (mol)}}{\text{EPS (mol)}}$$

$$(c) \text{ Degree of UA grafting (\%)} = \frac{\text{Number of UA grafted}}{\text{Number of UA per chain}^d} \times 100 \%$$

$$(d) \text{ Number of UA per chain} = \frac{M_n \text{ EPS (g/mol)}}{M \text{ repeating unit (g/mol)}} \times 3 \text{ UA in repeating unit} = 1701$$

$$(e) \text{ EPS in grafted EPS-pNIPAM (\%)} = \frac{\text{EPS (mg)}}{\text{EPS (mg)} + \text{grafted pNIPAM (mg)}} \times 100\%$$

Table 2. Characterization of grafted EPS-pNIPAM polymers in terms of the reaction efficiency (see eq. a), the number of UA grafted (see eq. b), the degree of UA grafting (see eq. c) and EPS amount in grafted EPS-pNIPAM polymers (see eq. e). The “Degree of UA grafting” values were used for sample designation, as referred in Table 1 (EPS-pX-Y%).

		Grafting characteristics										
Reaction condition	Polymer	EPS (mg)	EPS (mol)	Initial pNI PA M (mg)	Final product (mg)	Free pNI PA M (mg)	Grafted pNI PA M (mg)	Grafted pNI PA M (mol)	Reaction efficiency (%) ^(d)	Number of UA grafted (b)	Degree of UA grafting (%) ^(c)	EPS/ EPS - pNI PA M (%) ^(e)
1	EPS-p5-16%	10	1.1 x 10 ⁻⁸	161	113 ± 2	86.3 ± 1	16.7 ± 1	3.0 x 10 ⁻⁶	10.4 ± 1.0	273 ± 20	16.1 ± 1.2	37 ± 2
2	EPS-p5-8%	20	2.2 x 10 ⁻⁸	200	143 ± 3	106 ± 1	16.1 ± 1	2.9 x 10 ⁻⁶	8.1 ± 0.7	132 ± 12	7.8 ± 0.7	55 ± 1
3	EPS-p5-3%	40	4.4 x 10 ⁻⁸	200	166 ± 4	113 ± 1	12.3 ± 1	2.2 x 10 ⁻⁶	6.2 ± 0.7	50 ± 6	3.0 ± 0.4	76 ± 1
4	EPS-	40	4.4 x 10 ⁻⁸	120	120	71.8	8.2	1.5	6.8 ± 0.8	34	2.0	83 ±

	p5-2%		4 x1 0 ⁻⁸		± 4	± 2	± 1	x10 ⁻⁶		± 4	± 0.2	1
4*	EPS- p5-0%	40	4. 4 x1 0 ⁻⁸	120	122 ± 2	82.0 ± 2	0	0	0	0	0	-
5	EPS- p20- 6%	5	5. 6 x1 0 ⁻⁹	151	107 ± 5	91.0 ± 1	11.1 ± 2	5.6 x10 ⁻⁷	7.4 ± 1.2	100 ± 18	5.9 ± 1.0	31 ± 2
6	EPS- p20- 3%	10	1. 1 x1 0 ⁻⁸	161	112 ± 1	91.3 ± 1	10.7 ± 2	5.4 x10 ⁻⁷	6.6 ± 1.1	48 ± 9	2.8 ± 0.5	48 ± 2
7	EPS- p20- 1%	20	2. 2 x1 0 ⁻⁸	200	157 ± 1	128. 0 ± 1	8.9 ± 2	4.5 x10 ⁻⁷	4.5 ± 1.2	20 ± 6	1.2 ± 0.4	69 ± 2
8	EPS- p20- 0.2%	20	2. 2 x1 0 ⁻⁸	120	105 ± 1	83.4 ± 1	1.6 ± 1	8.0 x10 ⁻⁸	1.3 ± 1.3	4 ± 4	0.2 ± 0.2	93 ± 2

Mn p5, 5,500 g/mol; Mn p20, 20 000 g/mol; Mn EPS, 900 000 g/mol; M repeating unit of EPS, 1587 g/mol with 3 UA residues (sodium salt).

For grafted EPS-p5 samples, the lowest amount of pNIPAM (8.2 mg) was grafted in EPS-p5-2%. By taking into account that 1701 UA are available for grafting per polysaccharide chain, it can be estimated that ~ 34 UA (2% of UA grafted) were efficiently functionalized, which corresponds to 34 pNIPAM chains grafted on one polysaccharide chain. In contrast, the highest amount of pNIPAM (16.7 mg) with ~ 273 pNIPAM chains (16% of UA grafted) was grafted in EPS-p5-16%. In EPS-pNIPAM polymers, EPS content varied from 37% for EPS-p5-16% to 83% for EPS-p5-2% prepared using the lowest (0.65) and the highest (3.5) COOH/NH₂ molar ratio, respectively (Table 1). For EPS-p20, a four-fold increase in pNIPAM chain length had no significant impact on both reaction efficiency and degree of grafting, when compared to EPS-p5 samples obtained using similar COOH/NH₂ molar ratios (Tables 1 and 2). Indeed, between 5.9% and 1.2% of UA were grafted for EPS-p20-6% and EPS-p20-1%, respectively. The lowest amount of grafted pNIPAM (1.6 mg) was obtained for EPS-p20-0.2%. In EPS-p20 samples, EPS content evolved between 51% and 93% for highly and slightly grafted EPS, respectively (Table 2).

Furthermore, FI-AF4-MALLS analysis allowed the determination of the molecular characteristics of EPS-pNIPAM samples, such as the molecular weight, the radius of gyration (R_g) and the chain conformation (Table 3). For molecular weight determination, dn/dc refractive index increment of pure EPS was used since the presence of free (ungrafted) pNIPAM in the samples prevented the estimation of the exact value for grafted polysaccharides. Nevertheless, an important increase in M_w was observed for both EPS-p5 and EPS-p20 samples (M_w > 10⁸

g/mol) together with a five-fold increase in R_g (~500 nm), when compared to starting infernan displaying M_w of 1.6×10^6 g/mol and R_g of ~100 nm. This increase was much higher than the simple addition of pNIPAM chains on the infernan backbone. In contrast, no increase in molecular weight was observed for EPS-p20-0.2%, having only 4 pNIPAM chains grafted on the polysaccharide backbone. Any increase was neither measured for ungrafted EPS-p5-0%, obtained by mixing EPS and pNIPAM without adding the coupling agent EDC/NHS, despite the presence of free (ungrafted) pNIPAM not completely removed during dialysis. Therefore, the increase in the molecular weight in EPS-pNIPAM samples resulted from inter-chain associations between polysaccharide chains mediated by grafted pNIPAM, which led to the formation of large aggregates. Free pNIPAM embedded within the sample was not involved in the formation of inter-chain associations since no increase in the molecular weight was observed in the ungrafted sample (EPS-p5-0%).

In addition, the hydrodynamic coefficient ν calculated from the slope of the log-log plot of the R_g as a function of the molecular weight indicated a change in molecular conformation upon grafting (Table 3). Indeed, a random coil conformation was observed for pure EPS (0.73), EPS mixed with pNIPAM (EPS-p5-0%) (0.68) and EPS-p20-0.2% (0.51) having only 4 pNIPAM chains grafted. In contrast, a net decrease in the hydrodynamic coefficient by one order of magnitude was noticed for EPS-p5 samples (from 0.02 to 0.06) and EPS-p20 (from 0.05 to 0.22), indicating a dense spherical structure in solution. The intermediate hydrodynamic coefficient obtained for EPS-p20-1% (0.22) could suggest mixed random coil/spherical conformation, most likely due to a very low amount of grafted pNIPAM, being critical for establishing inter-chain associations.

Table 3. Characterization of grafted EPS-pNIPAM polymers in terms of their weight-average molecular weight (Mw), radius of gyration (Rg) and hydrodynamic coefficient (ν).

		Molecular characteristics		
Reaction condition	Polymer	Mw (g/mol)	Rg (nm)	ν
-	EPS	$1.6 \pm 0.1 \times 10^6$	104 ± 4	0.73
-	pNIPAM (p5/p20)	$1.0 \pm 0.1 \times 10^5$	67 ± 3	-
1	EPS-p5-16%	$9.0 \pm 0.6 \times 10^7$	482 ± 5	0.06
2	EPS-p5-8%	$8.2 \pm 0.6 \times 10^7$	471 ± 5	0.02
3	EPS-p5-3%	$1.3 \pm 0.1 \times 10^9$	503 ± 5	0.04
4	EPS-p5-2%	$1.3 \pm 0.1 \times 10^9$	510 ± 5	0.05
4*	EPS-p5-0%	$1.2 \pm 0.1 \times 10^6$	99 ± 7	0.68
5	EPS-p20-5%	$3.0 \pm 0.3 \times 10^8$	448 ± 4	0.09
6	EPS-p20-3%	$1.0 \pm 0.1 \times 10^9$	491 ± 5	0.05
7	EPS-p20-1%	$9.0 \pm 0.9 \times 10^8$	490 ± 5	0.22
8	EPS-p20-0.2%	$1.2 \pm 0.1 \times 10^6$	214 ± 4	0.51

Even though MD simulations showed that all UA on the infernan backbone and its side chain could be grafted, the pNIPAM functionalization was incomplete. It required pNIPAM molar excess to improve the reaction efficiency (<10% for EPS-p5 and <7% for EPS-p20, Table 2) by increasing the probability of encounter between amino-terminated pNIPAM and EDC/NHS-activated polysaccharide carboxylic acid groups. It can be thought that the grafting of one pNIPAM chain may preclude the grafting of another chain due to steric hindrance and lower accessibility of neighboring UA. Moreover, the molecular weights of the two pNIPAM (p5 and

p20) in an aqueous solution were much higher ($\sim 100,000$ g/mol) (Table 3) when compared to the molecular weight determined in an appropriate solvent and given by the supplier (5,500 g/mol for p5 and 20,000 g/mol for p20). Therefore, in agreement with MD simulations, pNIPAM chains tended to aggregate below LCST, thus forming clusters, as previously reported by Yan, Huang, Zhang, & Zhou (2015). This aggregation, on the one hand, limited pNIPAM grafting on the EPS and on the other hand, prevented unreacted pNIPAM from complete elimination by dialysis through a 50,000 g/mol cut-off membrane. Even if several studies reported on anionic polysaccharides grafted with pNIPAM, only a few of them determined the degree of UA grafting. Safakas *et al.* (2021) grafted 3 pNIPAM chains (23,000 g/mol) per alginate chain (140,000 g/mol), while Guo *et al.* (2018) functionalized one alginate chain (60,000 g/mol) with 2 pNIPAM chains (14,000 g/mol). However, no information about free (ungrafted) pNIPAM eventually remaining in the sample was reported in these different studies.

3.2.2. Band assignment in grafted EPS by Attenuated Total Reflection Fourier Transform Infrared (ATR-FTIR) spectroscopy

Native EPS, pNIPAM and grafted EPS-pNIPAM polymers were analyzed using ATR-FTIR spectroscopy. EPS-p5 and EPS-p20 spectra are shown in Fig. 3. EPS-p20 spectra are presented in Fig. S4. The absorption regions of interest agree with the vibrational bands first described by Ragu n s *et al.* (1997). A wide absorption band around 3310 cm^{-1} and a weak band around 2920 cm^{-1} were associated, respectively, with O-H and C-H stretching vibrations. Two strong absorptions at 1600 cm^{-1} and 1408 cm^{-1} were attributed to carboxylate groups asymmetric and symmetric stretching vibrations. The absorption band around 1350 cm^{-1} was assigned to the deformation vibrations C-H₂/C-H₃ and C-OH. The band at 1220 cm^{-1} confirmed the presence of sulfate groups. The band around 1016 cm^{-1} coincided with the C-O stretching vibrations of the

polysaccharide pyranose rings. The ATR-FTIR spectrum of p5 has the characteristic peaks of the pNIPAM. The absorption band around 3300 cm^{-1} was associated with the N-H stretching vibration. The amide I (1635 cm^{-1}), amide II (1535 cm^{-1}) and amide III ($1170\text{-}1130\text{ cm}^{-1}$) bands were characteristic of the C=O, N-H deformation and C-N stretching vibrations, respectively. Finally, the asymmetric and symmetric deformation vibrations C-H₂/C-H₃ were also present. The spectra of grafted polysaccharides have a similar absorption profile as pNIPAM alone. Those of pNIPAM hid the EPS bands except at 1016 cm^{-1} , where the decrease in the pyranose ring band was observed, in accordance with the weight proportion of EPS within each final polymer. No new absorption band attesting EPS grafting with pNIPAM was observed, as the coupling reaction leads to the formation of an amide bond, already present within the repeating unit of pNIPAM-NH₂. Indeed, one chain of pNIPAM possesses 48 amide functions, while 176 functions are present in the p20 chain. The grafting will therefore have a very low impact on the intensity of the amide band. Although, the influence of EPS/pNIPAM weight ratio in the spectra of resulting EPS-pNIPAM polymers was observed, it was not possible from ATR-FTIR spectra to distinguish between grafted and free pNIPAM. Indeed, ATR-FTIR spectrum of EPS-p5-2% overlaid with that of ungrafted EPS-p5-0%.

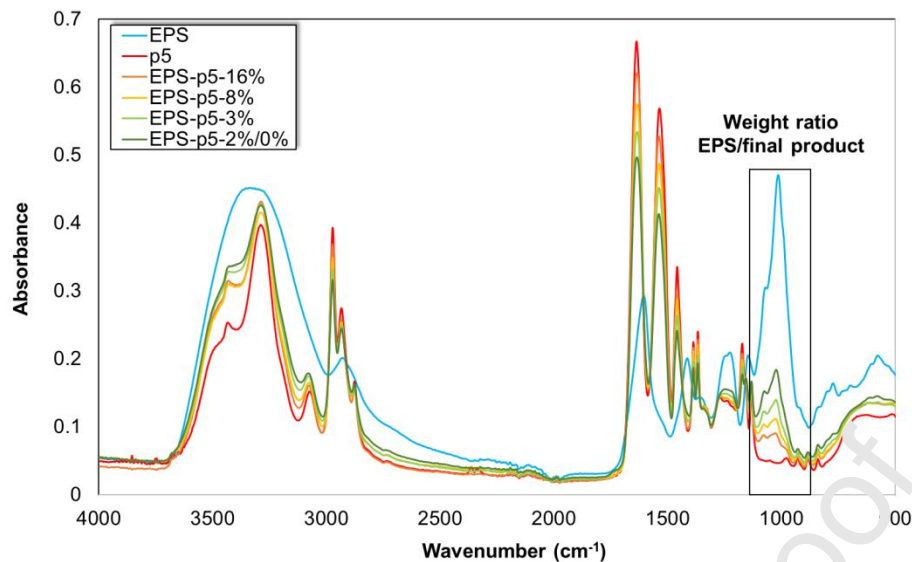


Fig. 3. ATR-FTIR spectra of EPS, p5 and EPS-p5 samples

3.2.3. Grafting assignment between EPS and pNIPAM chains by Nuclear Magnetic Resonance (NMR)

In order to get further insight into EPS-pNIPAM structure, NMR spectroscopy was applied to finely characterize the covalent grafting between the two polymers. ^1H -NMR spectra of EPS, p5 and the mixture thereof (EPS-p5-0%) as well as of the grafted polymer EPS-p5-2% were measured at 40°C - a temperature above pNIPAM LCST - as a higher definition of the peaks could be gained for protons located in a more rigid system (Coronado, Pekerar, Lorenzo, & Sabino, 2011). A comparison of the spectra clearly revealed an overwhelming predominance of the peaks related to p5 vs. EPS repeating unit (Fig. S5), as already observed for pNIPAM grafting to high molecular weight polysaccharides (Ciocoiu *et al.*, 2018; Coronado *et al.*, 2011; ter Boo, Richards, Moriarty, Grijpma, & Eglin, 2016). This could plausibly be to two major reasons: i) the higher number of p5 vs. EPS repeating units - approx. 48×34 vs. 567, respectively - as results by the ratio between M_n and repeating unit molecular weight of pNIPAM p5 (5,500

g/mol / 113 g/mol = 48), the number of UA grafted to a pNIPAM chain in EPS-p5-2% sample (34, see Table 2) and the ratio between Mn and repeating unit molecular weight of EPS (900,000 g/mol / 1587 g/mol = 567; see Table 1); ii) a shorter transverse relaxation time of the polysaccharide chain caused by a markedly lower overall tumbling associated with its much higher length. In order to gain more insights into the covalent linkage between the polymers, a ^1H , ^1H -homonuclear and a ^1H , ^{13}C -heteronuclear 2D-NMR spectrum (COSY and DEPT-HSQC, respectively) were measured for the samples. The attention was focused on the region of the spectra between approx. 2.5 and 3.5 ppm, where the ^1H signals of the methylene groups of the aminoethanthal (NH₂CH₂CH₂S, indicated as e and f in Fig. 4) moiety at p5 terminal end are located (Lima *et al.*, 2021). In particular, CH₂N and CH₂S groups were found to resonate at $\delta_{\text{H/C}}$ 3.19/39.6 and 2.82/30.1 ppm (f and e signal, respectively), in the spectrum of both p5 alone and its mixture with the polysaccharide (EPS-p5-0%) (Fig. 4), thus revealing that any ionic interaction between the amine and the carboxyl groups of the two polymers had no effect on the chemical shift of the aminoethanthal moiety. Conversely, a downfield shift of the ^1H chemical shift value related to the CH₂N group was found in the spectra of the grafted polymer EPS-p5-2%, in agreement with the presence of an electron-withdrawing moiety linked to the nitrogen atom, *i.e.* a carboxyl group forming an amide bond (Chen, Pawar, Munot, Chen, & Hsu, 2005). Moreover, both the single signals of CH₂N and CH₂S (indicated in Fig. 4 as f' and e', respectively) in p5 and EPS-p5-0% DEPT-HSQC spectra split into three different signals in EPS-P5-2% spectrum, thus suggesting that the amidoethanthal (CONHCH₂CH₂S)CH₂ atoms are divided into three different chemical environments. This could be ascribed to an effect of the CO groups involved in the amide linkages, located on three different UA units of EPS repeating unit.

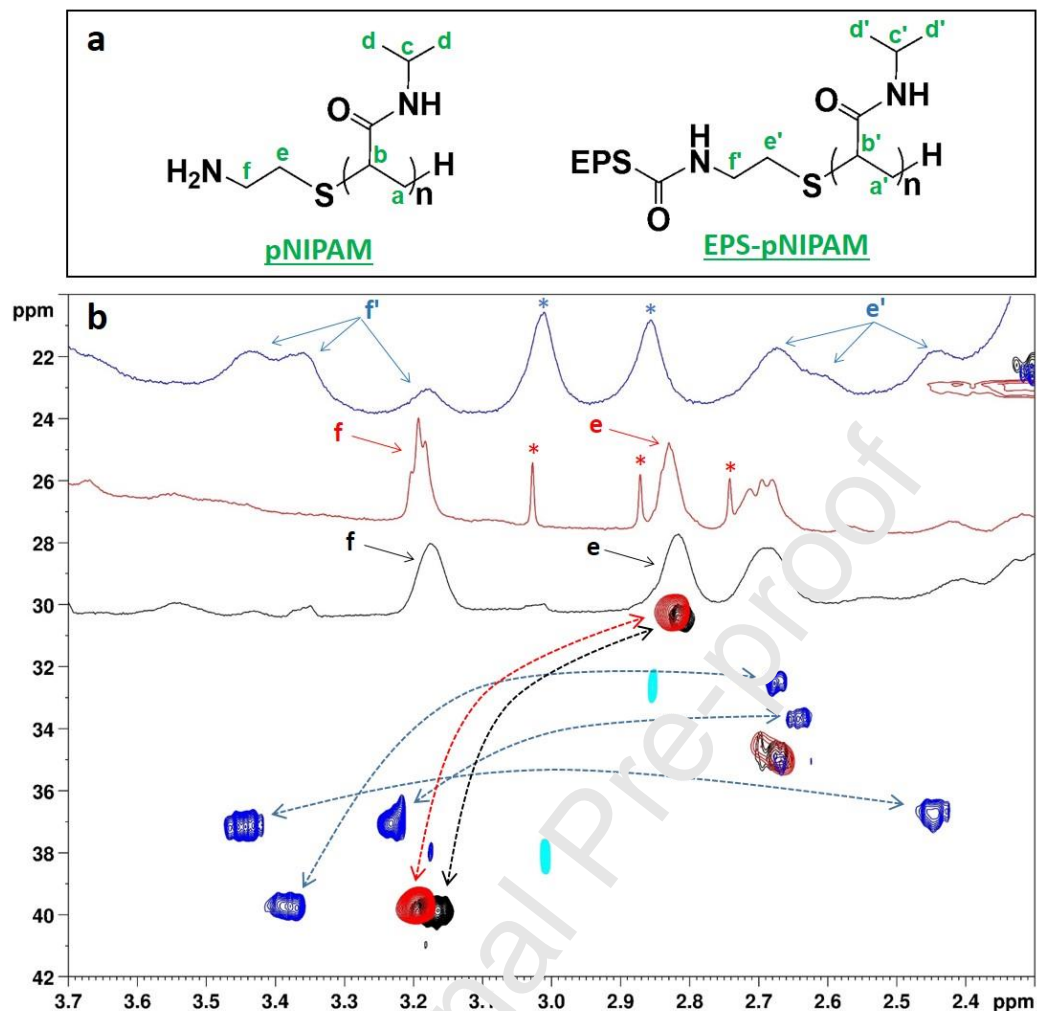


Fig. 4. (a) Chemical structure of free and EPS-grafted pNIPAM and (b) zoomed region of ^1H and ^1H , ^{13}C -DEPT-HSQC NMR spectra (600 MHz, D_2O , 40°C) of p5 (black), EPS-p5-0% (red) and EPS-p5-2% (blue) samples (CH₂ groups in black, red and blue, CH and CH₃ groups in grey, orange and light blue in the DEPT-HSQC spectra of p5, EPS-p5-0% and EPS-p5-2%, respectively). Signals marked with an asterisk are related to low molecular weight contaminants as demonstrated by their absence in diffusion-ordered ^1H -NMR spectra (DOSY, see Fig. S6). Arrows connect signals related to protons on adjacent carbon atoms, as revealed by COSY spectra (see Fig. S7-S9). Full ^1H and ^1H , ^{13}C -DEPT-HSQC NMR spectra are reported in Fig. S5 and S10-S12, respectively.

3.3. Thermosensitive properties characterization of grafted infernan.

Thermosensitive properties of EPS-pNIPAM were studied to assess if grafted pNIPAM chains could induce phase transition of the whole polymer. Indeed, the heat-sensitive nature of pNIPAM was described at the molecular level by its ability to adopt a temperature-dependent structural change involving a coil-to-globule transition. At room temperature, pNIPAM chains adopt a random-coil conformation: hydrogen bonds between water molecules and amide groups promote the establishment of a hydration layer around nonpolar surfaces in the form of a cage responsible for the solvation of hydrophobic isopropyl groups. The increase in temperature generates a change in the enthalpy/entropy balance, thus destabilizing this molecular network: polymer-polymer interactions are favored to the detriment of water-polymer interactions. As a result, pNIPAM chains collapse to minimize contact between hydrophobic surfaces of pNIPAM and water, thus adopting a thermodynamically stable globular conformation (Deshmukh, Sankaranarayanan, Suthar, & Mancini, 2012; Fujishige, Kubota, & Ando, 1989; Ono & Shikata, 2006; Tavagnacco *et al.*, 2018).

3.3.1. LCST determination in semi-diluted solutions of grafted infernan

The evolution of absorbance as a function of temperature in semi-diluted EPS-pNIPAM polymer solutions was investigated (Fig. 5). At room temperature, all solutions prepared at 1 mg/mL were transparent and no absorbance was measured. Turbidity started to increase at 32°C with a progressive increase in absorbance up to 38°C. The change from transparent to opaque appearance at 32°C resulted from the phase transition induced by the association of polysaccharide chains through grafted pNIPAM, thus showing a thermosensitive nature of grafted infernan. Indeed, in semi-dilute solutions above LCST, intra-chain folding and inter-

chain associations between pNIPAM chains occur, where the grafted chains create micelle-like aggregates, acting as physical crosslinks (Guo *et al.*, 2015; Mortisen, Peroglio, Alini, & Eglin, 2010; Petit, Karakasyan, Pantoustier, & Hourdet, 2007). However, it cannot be excluded that the presence of residual, free pNIPAM in EPS-pNIPAM samples contributes to the overall increase in absorbance, in particular for EPS with a low degree of grafting, displaying similar absorbance evolution between ungrafted EPS-p5-0% and slightly grafted EPS-p5-2% (Fig. 5A). The LCST of grafted infernan was close to pure pNIPAM (32°C), as reported for other pNIPAM grafted polysaccharides, such as alginate (Vasile & Nita, 2011), hyaluronic acid (Chen & Cheng, 2009) and pullulan (Constantin, Bucătariu, Stoica, & Fundueanu, 2017). Similar thermosensitive properties with LCST at 32°C were observed for EPS-p20 (Fig. 5B). However higher absorbance was measured due to longer pNIPAM chains.

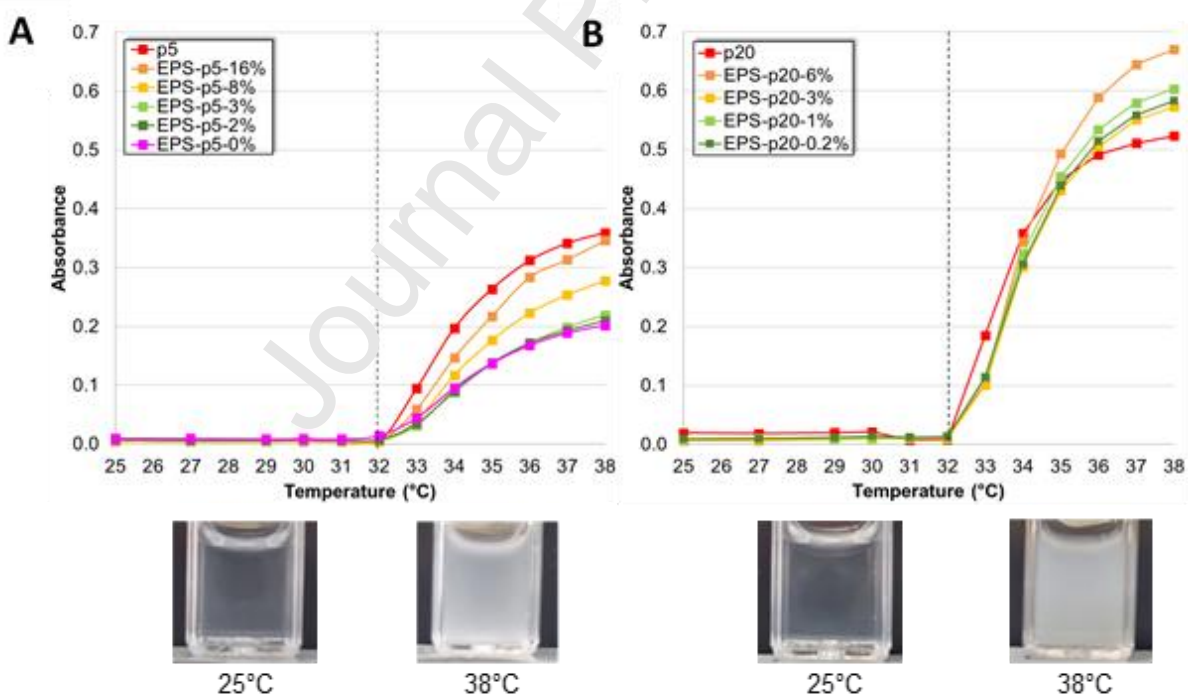


Fig. 5. Evolution of absorbance at 550 nm with temperature for semi-diluted solutions of (A) pNIPAM p5 and EPS-p5, and (B) p20 and EPS-p20 at 1 mg/mL in PBS pH 7.4.

3.3.2. Determination of hydrodynamic diameter of grafted infernan by Dynamic Light Scattering (DLS)

DLS measurements were applied to determine the impact of temperature on the hydrodynamic diameter of EPS-pNIPAM polymers in semi-dilute solutions at 1 mg/mL in PBS pH 7.4. DLS analysis was carried out in triplicate on three independently synthesized samples and the average profiles were displayed in Fig. 6, since very low standard deviation values were measured (Table S4). Indeed, these three independently synthesized samples were obtained with similar yields with very low standard deviation values (Table 2).

Below LCST, at 25°C, a major population of ~100 nm was present for pure pNIPAM (p5 or p20) (Fig. 6A, B), together with a population of ~200 nm, resulted most likely from the association of pNIPAM chains, as already observed by FI-AF4-MALLS-dRI. Above LCST, at 38°C, only one pNIPAM population of ~2200 nm was measured, indicating aggregation of chains induced by rearrangement of water in the proximity of the polymer surface with hydrophobic interactions becoming dominant (Ortiz de Solorzano *et al.*, 2020; Tavagnacco *et al.*, 2018). Similar DLS results for free pNIPAM below and above LCST were reported by Yan *et al.*, (2015). In contrast, pure EPS did not present any thermoresponsive properties, as the hydrodynamic diameter of its major population of ~700 nm remained unchanged below and above LCST (Fig. 6A).

Below LCST at 25°C, in the case of EPS-p5 polymers, four populations were observed (Fig. 6C), with the major one corresponding most likely to grafted EPS with the hydrodynamic diameter varying from 753 ± 101 nm for the most grafted EPS (EPS-p5-16%) to 1500 ± 56 nm for the less grafted EPS (EPS-p5-2%) (Table S4). Other populations of lower intensities

indicated most likely aggregated chains of free pNIPAM, remaining in the samples. The increase in the hydrodynamic diameter for grafted EPS of decreasing grafting degree was independent from the pNIPAM grafting and was due to the increasing amount of the polysaccharide per sample (all prepared at 1 mg/mL), since the EPS amount in grafted EPS-pNIPAM increased when the degree of UA grafted decreased (Table 2). With increasing EPS concentration, inter-chain interactions between polysaccharide chains mediated by grafted pNIPAM increased, which led to higher hydrodynamic diameters (Fig. 6G). Indeed, when EPS-pNIPAM solutions were prepared at constant EPS concentration (0.1 mg/mL), similar diameters of ~1000 nm were measured for grafted EPS (EPS-p5-8%, 3%, 2%) (Fig. S13, Table S5). They were significantly higher than pure EPS (~300 nm), emphasizing that inter-chain interactions mediated by grafted pNIPAM are responsible for EPS association. The most grafted EPS sample (EPS-p5-16%) showed lower diameter of ~700 nm compared to less grafted EPS. In this sample, due to high degree of grafting, inter-chain interactions resulted in a more compact network. Ungrafted EPS-p5-0% sample, corresponding to EPS with remaining free pNIPAM, displayed slightly lower diameter compared to grafted EPS samples (Fig. 6C and S13, Tables S4 and S5). In this particular case, no inter-chain interactions through grafted pNIPAM could be established between polysaccharide chains, which limits their ability of association.

Similar results were obtained for grafted EPS-p20 polymers below LCST, where the hydrodynamic diameter increased with increasing amount of polysaccharide within the grafted samples due to increasing inter-chain interactions, except for the EPS-p20-0.2%, having the lowest number of grafted pNIPAM chains (Fig. 6D and S13, Tables S4 and S5). In this case, the inter-chain interactions could not be efficiently established due to the low level of EPS grafting. Ungrafted EPS-p20-0% showed similar behavior to EPS-p20-0.2% and ungrafted EPS-p5-0%

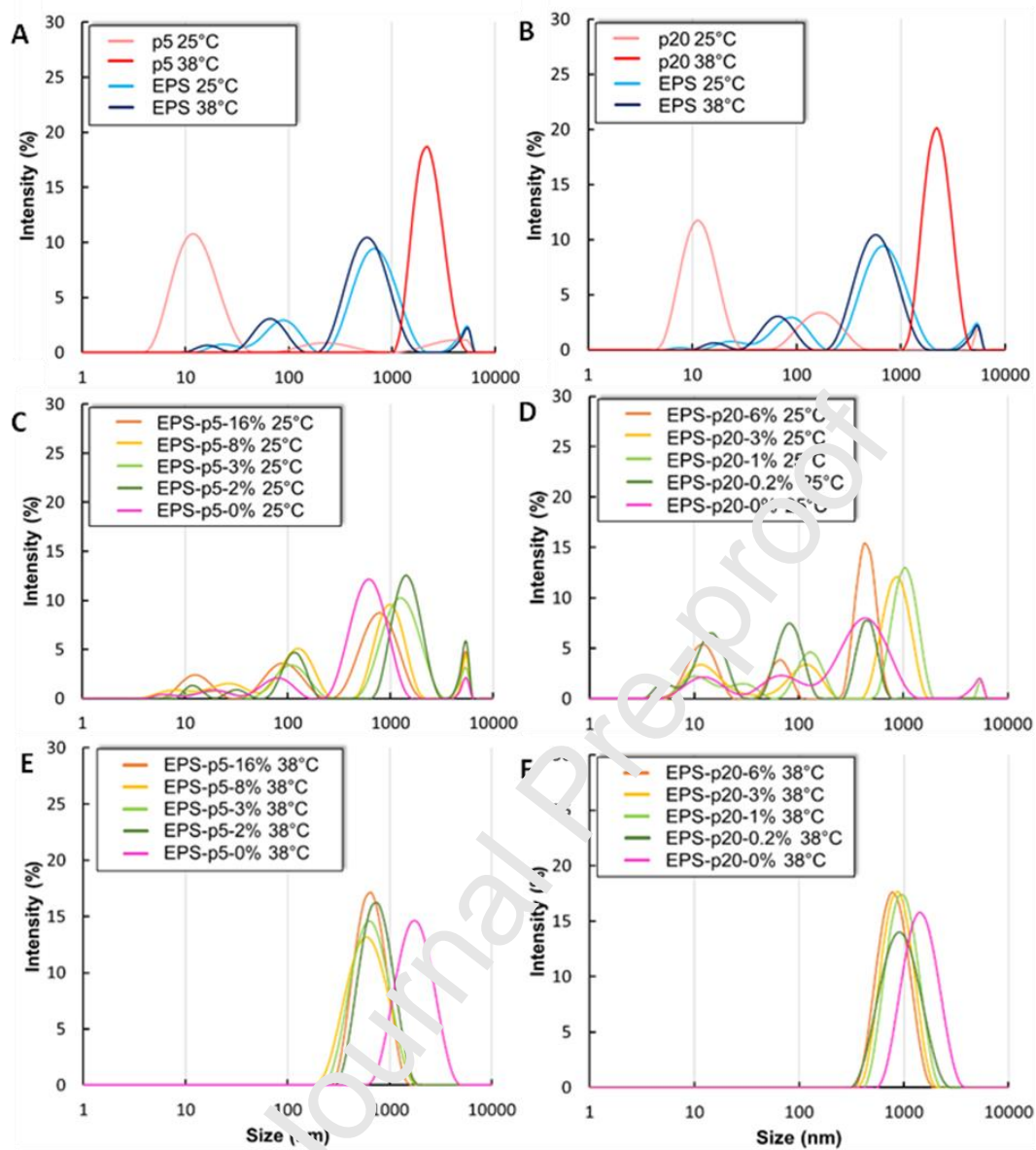
sample. DLS measurements below LCST are consistent with FI-AF4-MALLS data showing the presence of large aggregates in grafted EPS samples resulting from inter-chain interactions (Table 3).

Above LCST at 38°C, a decrease in hydrodynamic diameter was observed for all grafted EPS-p5 samples with the presence of only one population between ~600 nm and ~800 nm in diameter, independently from the EPS grafting degree and EPS concentration (Fig. 6E and S13, Tables S4 and S5). This single population results from the aggregation of all populations present at 25°C, mediated by inter-chain interactions involving grafted pNIPAM chains. This further induces a decrease in the diameter size due to folding of grafted polysaccharide chains, allowing a more compact structure to be adopted (Fig. 6G). Such a chain collapse was also observed by DLS for alginate (Vasile & Nita 2011), galactan (Lima *et al.* 2021) and dextran (Carneiro *et al.* 2021) once grafted with pNIPAM. The similar diameter size of the samples despite different grafting degrees and EPS concentrations could be due to high EPS to pNIPAM molecular weight ratio. Indeed, the resulting size will be governed by the polysaccharide chain length, while the grafted pNIPAM chains play the role of actuator by inducing the collapsed state through EPS chain folding. For the ungrafted EPS (EPS-p5-0%), the higher diameter (~1900 nm) observed compared to the grafted EPS-p5 may result from less dense network formed by polysaccharide chains in the absence of inter-chain interactions mediated by pNIPAM. In this case, aggregation of free pNIPAM chains, embedded within the polysaccharide chains, resulted in the final measured diameter being close to that of pure pNIPAM p5 (~2200 nm).

Similar results were observed for grafted EPS-p20, where only one population of ~ 900 nm in diameter was measured regardless of the degree of EPS grafting (Fig. 6F and Table S4). In contrast to grafted EPS-p5, the chain collapse was less pronounced at 38°C due most likely to

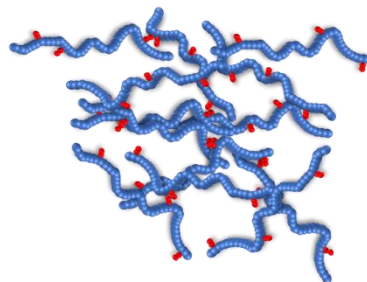
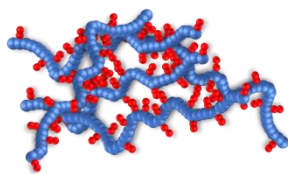
their lower degree of grafting. When compared to grafted EPS-p20 samples, higher diameter was measured for ungrafted EPS-p20-0% (~1300 nm), in a similar manner to EPS-p5-0%.

Finally, DLS measurements show that the grafted polysaccharide chains possess thermosensitive properties responsible for network structuring, as different behaviors were observed between grafted EPS-pNIPAM (p5 and p20) and EPS containing only free pNIPAM (EPS-p5-0% and EPS-p20-0%).

**G** Highly grafted EPS-pNIPAM

Slightly grafted EPS-pNIPAM

Below LCST



Above LCST

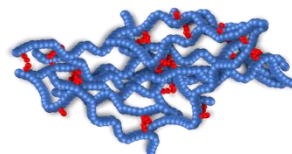
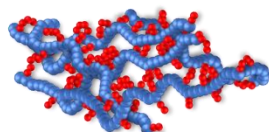


Fig. 6. Impact of the temperature (below and above LCST) on the hydrodynamic diameter of semi-diluted solutions (1 mg/mL): (A) EPS and pNIPAM p5 at 25°C and 38°C, (B) EPS and pNIPAM p20 at 25°C and 38°C, (C) EPS-p5 at 25°C, (D) EPS-p20 at 25°C, (E) EPS-p5 at 38°C, and (F) EPS-p20 at 38°C. (G) Schematic representation of semi-diluted EPS-pNIPAM solutions below and above LCST for two extreme cases (with respect to the degree of grafting and EPS amount in the grafted samples) showing the effect of inter-chain interactions between EPS chains mediated by grafted pNIPAM on resulting polymer diameters: highly grafted EPS-pNIPAM (EPS-p5-16%) having 16 pNIPAM chains (in red) per EPS chain and 5 EPS chains (in blue) and slightly grafted EPS-pNIPAM (EPS-p5-3%) with 3 pNIPAM chains (in red) per EPS chain and 13 EPS chains (in blue).

3.3.3. Investigation of chain morphology in grafted infernan by Atomic Force Microscopy (AFM)

AFM imaging in intermittent contact mode in the air was applied to investigate the morphology of infernan chains grafted with pNIPAM below and above LCST. Imaging was performed on highly diluted samples to avoid aggregation. To assess the polysaccharide chain morphology below and above LCST, aqueous solutions of EPS, pNIPAM (p5 and p20) and EPS-pNIPAM samples at 1 mg/mL were incubated at 25°C and 37°C, respectively, before being diluted at 5 µg/mL in water (maintained either at 25°C or 37°C). Although all samples were prepared at the same concentration, the amount of EPS in grafted samples increased inversely to grafting density (Table 2). Before imaging, samples were dried on a freshly cleaved mica surface at either 25°C or 37°C.

Below LCST, the morphology of grafted polysaccharide chains already differed from that

observed for pure EPS (Fig. 7A and S14). Chains appeared longer and highly connected with a slight increase in diameter from 0.36 nm for pure EPS to 0.43 nm and 0.71 nm for EPS-p5-8% and EPS-p5-16%, mainly observed on branched parts. Similar results were obtained for EPS-p20 (Fig. 7B and S14), suggesting that at least two grafted polysaccharide chains could associate through pNIPAM chains (inter-chain associations). Above LCST, folded EPS chains were observed for the most grafted EPS-p5-16%. Although the experimental rate of grafting was lower (up to 16%) than in the MD simulations (down to 33%), the AFM image of the sample clearly illustrates the existence of local polysaccharide bending. This may reflect a non-regular distribution of pNIPAM branches along the infernan chain with increased local pNIPAM density. In agreement with MD simulations, pNIPAM inter-chain associations may induce the polysaccharide backbone bending in such fragments with a higher density of grafting. The local infernan compaction due to backbone bending would make possible the interactions of pNIPAM chains from remote regions of EPS with the resultant global chain folding. In addition to folded polysaccharide chains, free ungrafted pNIPAM chains associated in nanoparticles of 2.5 nm in diameter were also observed in the EPS-p5-16% sample (Fig. 7A and S14). No similar chain folding was observed above LCST, in the highly diluted conditions used, for other less grafted EPS-p5 and EPS-p20, where chain morphologies remained similar below and above LCST (Fig. 7A). Indeed, a considerably lower amount of UA functionalized with pNIPAM chains prevented most likely from intra-chain interactions, while favoring inter-chain associations. Polysaccharide chains were clearly branched, forming a highly connected network already in highly diluted solutions. For EPS-p20 samples above LCST, some nanoparticle assemblies were observed on the polysaccharide chains, corresponding most likely to micelle-like structures formed by grafted pNIPAM chains, allowing for the establishment of inter-chain associations, in agreement with

the previously proposed models (Guo *et al.*, 2015; Mortisen *et al.*, 2010; Petit *et al.*, 2007).

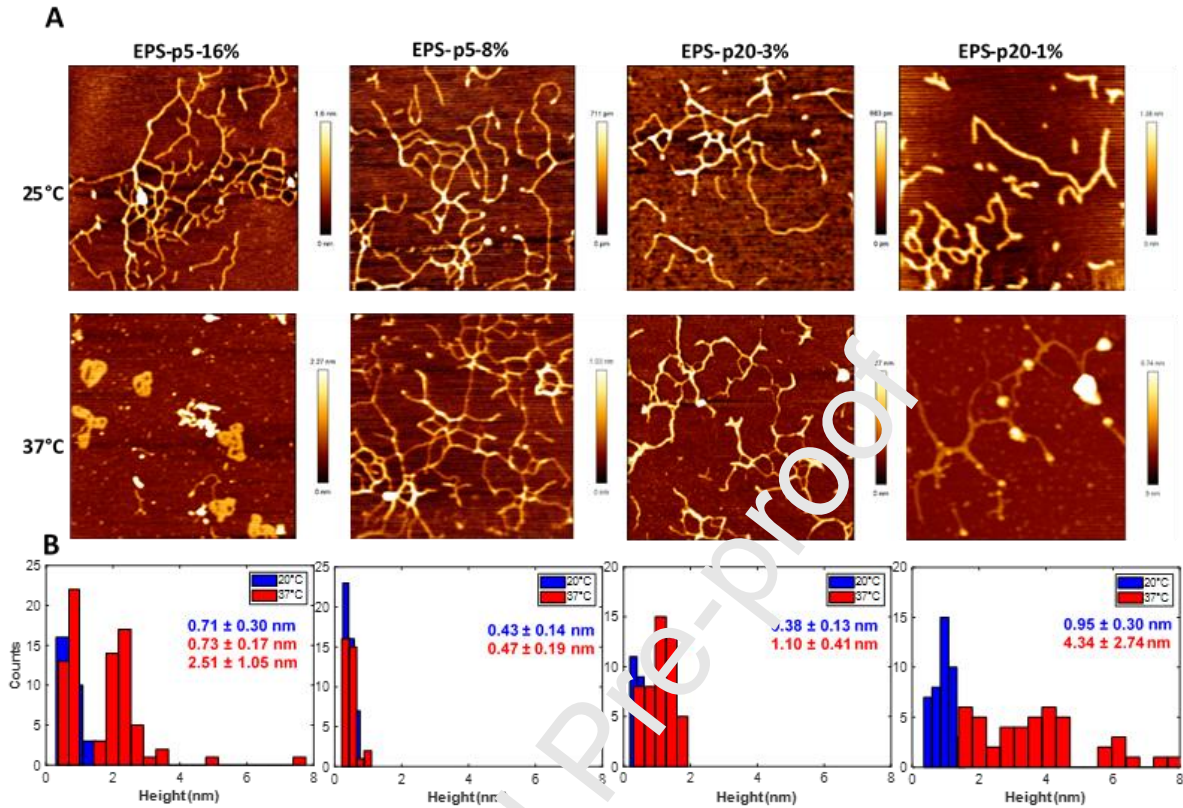


Fig. 7. (A) AFM height images (2 μm x 2 μm) obtained in intermittent contact in air and (B) height distribution of EPS-p5-16%, EPS-p5-8%, EPS-p20-3% and EPS-p20-1% at 25°C and 37°C.

3.4. Investigation of inter-chain EPS-pNIPAM associations by Monte Carlo simulations.

The Monte Carlo simulations were conducted to investigate the ability of grafted infernan chains to form an infinite network undergoing a sol-gel transition near the percolation, *i.e.* when at least one cluster formed a continuous path by connected chains from one side of a lattice to the opposite one. In these simulations performed on a two-dimensional square lattice of size L at 37°C, only attractive short-range interactions between grafted pNIPAM chains belonging to neighbouring polysaccharide chains were considered. Contrary to other Monte Carlo simulations

or the previous MD simulations where the analysis scale was atomic, molecular or at the single polymer chain level (Cornette, Ramirez-Pastor, & Nieto, 2003; Tzounis, Anogiannakis, & Theodorou, 2017), the elementary building block of these simulations was the EPS-p20 chain. Three snapshots of the same simulation were represented in Fig. 8A for different occupation probabilities ϕ of 0.03, 0.06 and 0.08, this latter corresponded to the percolation threshold. The simulation performed on a square lattice of 2 μm in size clearly showed the construction of the EPS-pNIPAM network with the formation of isolated clusters where neighboring polysaccharide chains were connected. All chains belonging to the same cluster were evidenced with the same colour and colours were related to the cluster size (*i.e.* the number of chains forming the cluster or the corresponding pixel number). As the size of the clusters increase with the number of chains deposited or ϕ , the neighbouring clusters progressively merge until percolation, where a continuous path of connected chains exists, crossing the lattice from one side to the opposite one. Interestingly, Monte Carlo simulations correctly described the inter-chain associations observed by AFM by considering similar polymer concentrations (Fig. 7). These simulations revealed that a percolated network of EPS-pNIPAM chains could be obtained by considering only attractive interactions between grafted pNIPAM chains belonging to neighboring EPS chains. Further Monte Carlo simulations were then carried out by varying the size of the square lattice, leading to the same qualitative result (Fig. S15).

The transposition of these Monte Carlo simulations to future experiments is not straightforward because simulations were carried out for finite lattice sizes, whereas experiments correspond to an infinite lattice. However, the extrapolation of the percolation threshold toward an infinitely large system (ϕ^∞) can be undertaken by a finite-size scaling analysis (Wu *et al.*, 2008). Indeed, the percolation probability curves as a function of ϕ , calculated from simulations for lattices of

different sizes, intersect at a single point corresponding to ϕ^∞ . Fig. 8B showed these curves obtained from simulations on lattices of increasing sizes: 1 μm , 2 μm , 5 μm and 10 μm . Increasing the lattice size makes the percolation probability curves steeper, which tend towards the limiting case of the Heaviside step function centered at ϕ^∞ for an infinite system. The Monte Carlo simulations estimate the percolation threshold for an infinitely large network of connected EPS-pNIPAM chains at 0.068. To remove the finite size effect of simulations, the occupation probability was normalized by $(\phi - \phi^\infty)L^\alpha$ where α is the critical exponent of the phase transition occurring in the studied system. Fig. 8C representing the percolation probability as a function of this reduced variable revealed that all the curves in Fig. 8B collapsed onto a single master curve. This result, with numerous points included in the collapsing curve, underlines that both the values of ϕ^∞ and α were accurately determined. In other words, the percolation threshold and critical exponent of EPS-pNIPAM networks were identical for various lattice sizes, revealing the universal character of the sol-gel transition near the percolation. Indeed, the α values were very close with 0.75, 0.77, 0.73 and 0.72 for the four simulated lattice sizes. Such finite-size scaling analysis was previously conducted to percolate particles or linear segments on two-dimensional lattices (Cornette *et al.*, 2005; Wu *et al.*, 2008). The percolation of these systems also belonged to the same universality class as that of random percolation models. Finally, the Monte Carlo simulations revealed that inter-chain interactions mediated by grafted pNIPAM chains are strong enough to form an infinite network of polysaccharide chains, a crucial feature in a hydrogel setting.

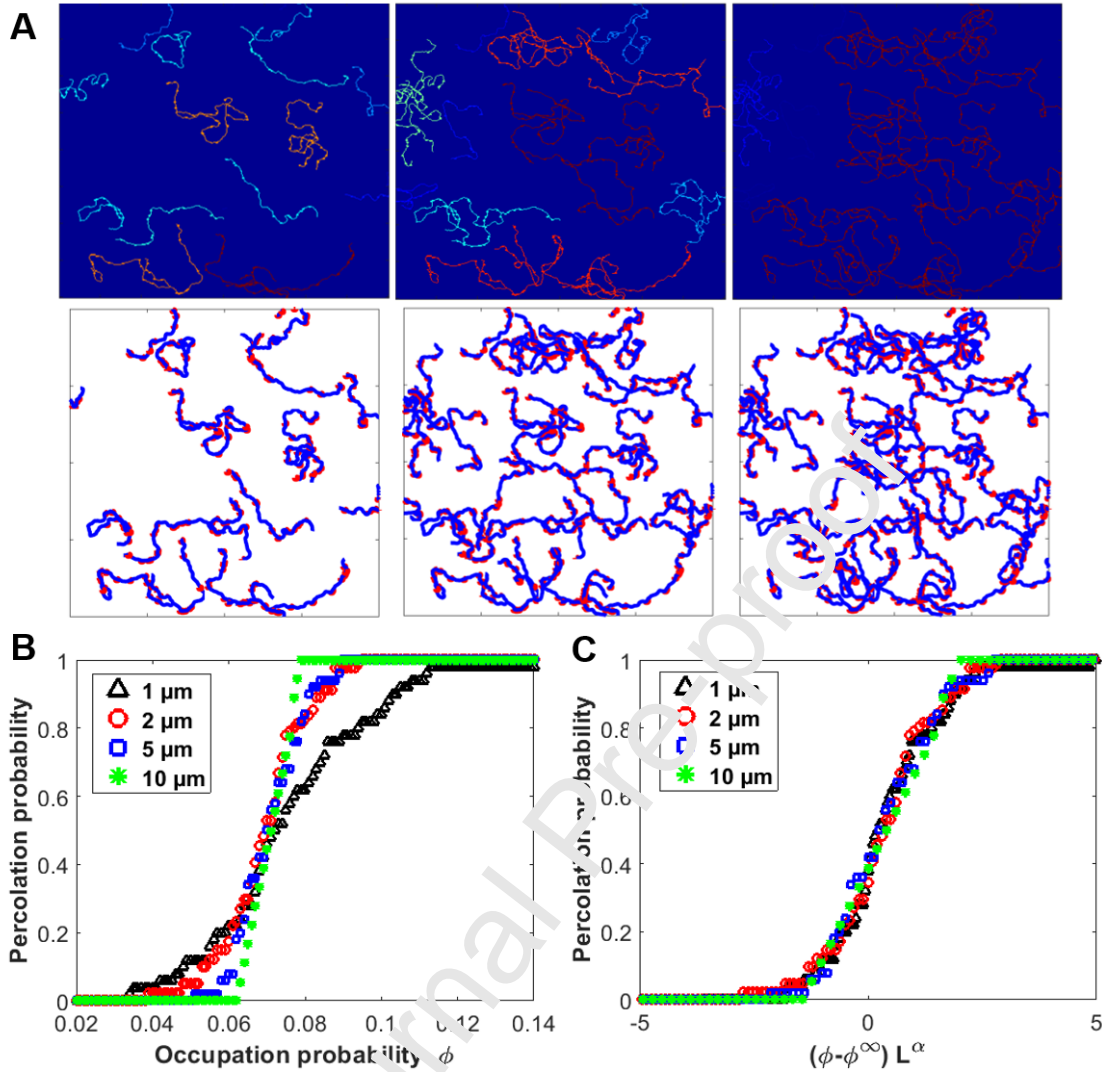


Fig. 8. (A) Snapshots of the Monte Carlo simulation on a square lattice of 2 μm showing the progressive formation of clusters from connected EPS-pNIPAM chains for different occupation probabilities of 3.1%, 6.2% and 8%. The same simulations showing EPS chains in blue and folded pNIPAM in red were presented below (for better visualization, the linewidth was increased by five-fold). (B) Percolation probability curves as a function of the occupation probability for different sizes of the square lattice. (C) Master curve of the percolation probability as a function of the normalized occupation probability.

4. Conclusion

In the present study, infernan, a marine bacterial EPS was grafted with pNIPAM with the aim of obtaining a thermosensitive polysaccharide that could further be used in tissue engineering as a hydrogel scaffold. Eight grafted polysaccharides were prepared by varying EPS/pNIPAM molar ratio as well as the molecular weight of pNIPAM. To describe their physicochemical characteristics, including the degree of grafting, molecular weight, chain conformation and morphology as well as their thermosensitive properties, an experimental approach was applied using several complementary techniques (FI-AF4-MALLS-dRI, ATR-FTIR, NMR, UV-Vis, DLS and AFM imaging). The covalent grafting between infernan and pNIPAM chains was finely characterized by NMR spectroscopy, while FI-AF4-MALLS-dRI allowed quantifying the grafting density. For grafted infernan samples, below LCST of $\sim 32^{\circ}\text{C}$, large aggregates resulting from inter-chain associations mediated by grafted pNIPAM were evidenced by FI-AF4-MALLS-dRI and DLS. Above LCST, the hydrodynamic diameter of grafted polysaccharides decreased (DLS), which led to more compact structures resulting from the rearrangement of water molecules in the vicinity of pNIPAM chains with hydrophobic interactions becoming dominant. A theoretical approach using MD simulations was applied to get further insight into molecular conformation of grafted infernan chains and their ability to establish intra and inter-molecular interactions. MD simulations showed the tendency of pNIPAM chains, when grafted to infernan, to interact with each other leading to the backbone bending. Such an intra-chain folding was clearly observed above LCST by AFM imaging for the most grafted sample (EPS-p5-16%) in highly-diluted solution. However, inter-chain associations were favored with lower grafting density, leading to a network of connected polysaccharide

chains (AFM imaging). A percolated network was also obtained by Monte Carlo simulations, which considered only the attractive interactions between grafted pNIPAM chains belonging to neighboring EPS chains. Therefore, this study shows that infernan can successfully be grafted with pNIPAM. The physicochemical and thermosensitive characteristics of grafted polysaccharides can be tuned by EPS/pNIPAM molar ratio and pNIPAM molecular weight, thus confirming the initial hypothesis. In the future, the ability of grafted infernan to form hydrogel scaffolds endowed with biological and mechanical properties for tissue engineering will be investigated.

Declarations of competing interest: The authors declare no conflict of interest.

Acknowledgments

The authors would like to thank Ifremer for PhD funding (A.F.). Financial support was provided by the French National Research Agency within the framework of the SmartIEs project (ANR-22-CE52-0005-01).

This research was funded by [ANR-22-CE52-0005-01]. A CC-BY public copyright license has been applied by the authors to the present document and will be applied to all subsequent versions up to the Author Accepted Manuscript arising from this submission, in accordance with the grant's open access conditions.



Author contribution

Arnaud Fillaudeau: Conceptualization, Methodology, Investigation, Formal analysis, Validation, Writing – Original Draft, Writing – Review & Editing; **Stéphane Cuenot:** Conceptualization, Methodology, Investigation, Formal analysis, Validation, Funding acquisition, Writing – Original Draft, Writing – Review & Editing; **Olga Makshakova:**

Conceptualization, Methodology, Investigation, Formal analysis, Writing – Original Draft, Writing – Review & Editing; **Serena Traboni**: Methodology, Investigation, Formal analysis, Writing – Original Draft; **Corinne Sinquin**: Methodology, Investigation, Formal analysis, Writing – Review & Editing; **Marie Hennetier**: Methodology, Investigation, Formal analysis, Validation, Writing – Review & Editing; **Emiliano Bedini**: Conceptualization, Methodology, Investigation, Formal analysis, Validation, Writing – Original Draft, Writing – Review & Editing; **Serge Perez**: Conceptualization, Methodology, Investigation, Formal analysis, Writing – Original Draft, Writing – Review & Editing; **Sylvia Collic-Jouault**: Conceptualization, Funding acquisition, Writing – Review & Editing; **Agota Zykwinska**: Conceptualization, Methodology, Investigation, Formal analysis, Validation, Funding acquisition, Writing – Original Draft, Writing – Review & Editing.

References

- Akoumany, K., Zykwinska, A., Sinquin, C., Marchand, L., Fanuel, M., Ropartz, D., Rogniaux, H., Pipelier, M., Delbarre-Ladrat, C., & Collic-Jouault, S. (2019). Characterization of new oligosaccharides obtained by an enzymatic cleavage of the exopolysaccharide produced by the deep-sea bacterium *Alteromonas infernus* using its cell extract. *Molecules*, *24*, 3441.
- Atoufi, Z., Kamrava, S. K., Davachi, S. M., Hassanabadi, M., Saeedi Garakani, S., Alizadeh, R., Farhadi, M., Tavakol, S., Bagher, Z., & Hashemi Motlagh, G. (2019). Injectable PNIPAM/hyaluronic acid hydrogels containing multipurpose modified particles for cartilage tissue engineering: Synthesis, characterization, drug release and cell culture study. *International Journal of Biological Macromolecules*, *139*, 1168-1181.
- Badri, A., Williams, A., Linhardt, R. J., & Koffas, M. A. (2018). The road to animal-free glycosaminoglycan production: Current efforts and bottlenecks. *Current Opinion in*

Biotechnology, 53, 85-92.

Baei, P., Daemi, H., Aramesh, F., Baharvand, H., & Eslaminejad, M. B. (2023). Advances in mechanically robust and biomimetic polysaccharide-based constructs for cartilage tissue engineering. *Carbohydrate Polymers*, 308, 120650.

Carneiro, M. J. M., Paula, C. B. A., Ribeiro, I. S., de Lima, L. R. M., Ribeiro, F. O. S., Silva, D. A., Araújo, G. S., Marinho Filho, J. D. B., Araújo, A. J., Freire, R. S., Feitosa, J. P. A., & de Paula, R. C. M. (2021). Dual responsive dextran-graft-poly (N-isopropylacrylamide)/doxorubicin prodrug via Schiff base reaction. *International Journal of Biological Macromolecules*, 185, 390-402.

Case, D. A., Ben-Shalom, I. Y., Brozell, S. R., Cerutti, D. S., Cheatham, III, T. E., Cruzeiro, V. W. D., Darden, T. A., Duke, R. E., Ghoreishi, L., Gilson, M. K., Gohlke, H., Goetz, A. W., Greene, D., Harris, R., Homeyer, N., Huang, Y., Izadi, S., Kovalenko, A., Kurtzman, T., Lee, T. S., LeGrand, S., Li, P., Lin, C., Liu, J., Muchko, T., Luo, R., Mermelstein, D. J., Merz, K. M., Miao, Y., Monard, G., Nguyen, C., Nguyen, H., Omelyan, I., Onufriev, A., Pan, F., Qi, R., Roe, D. R., Roitberg, A., Sagui, C., Schott-Verdugo, S., Shen, J., Simmerling, C. L., Smith, J., Salomon-Ferrer, R., Swails, J., Walker, R. C., Wang, J., Wei, H., Wolf, R. M., Wu, X., Xiao, L., York, D. M., & Kollman, P.A. (2018). AMBER 2018, University of California, San Francisco.

Celikkin, N., Rinoldi, C., Costantini, M., Trombetta, M., Rainer, A., & Świążkowski, W. (2017). Naturally derived proteins and glycosaminoglycan scaffolds for tissue engineering applications. *Materials Science and Engineering: C*, 78, 1277-1299.

Chen, J.-P., & Cheng, T.-H. (2009). Preparation and evaluation of thermo-reversible copolymer hydrogels containing chitosan and hyaluronic acid as injectable cell carriers. *Polymer*, 50, 107-116.

- Chen, C.-T., Pawar, V. D., Munot, Y. S., Chen, C.-C., & Hsu, C.-J. (2005). Diethylene glycol ether-linked 3,4,5-trihydroxybenzamides as triply branched dendritic anchors to CdSe/ZnS core/shell type nanoparticles: potential hydrophilic fluorescent probes. *Chemical Communications*, *19*, 2483-2485.
- Cimini, D., Bedini, E., & Schiraldi, C. (2023). Biotechnological advances in the synthesis of modified chondroitin towards novel biomedical applications. *Biotechnology Advances*, 108185.
- Ciocoiu, O. N., Staikos, G., & Vasile, C. (2018). Thermoresponsive behavior of sodium alginate grafted with poly(N-isopropylacrylamide) in aqueous media. *Carbohydrate Polymers*, *184*, 118-126.
- Colliec-Jouault, S., Esposito, F., Ledru, H., Siquin, C., Marchand, L., Fillaudeau, A., Routier, S., Buron, F., Lopin-Bon, C., Cuenot, S., Fednini, E. & Zykwinska, A. (2023). Glycosaminoglycan mimetics obtained by microwave-assisted sulfation of marine bacterium sourced infernan exopolysaccharide. *Biomacromolecules*, *24*, 462-470.
- Constantin, M., Bucătariu, S., Stoica, I. & Fundueanu, G. (2017). Smart nanoparticles based on pullulan-g-poly(N-isopropylacrylamide) for controlled delivery of indomethacin. *International Journal of Biological Macromolecules*, *94*, 698-708.
- Coronado, R., Pekerar, S., Lorenzo, A.T. & Sabino, M.A. (2011). Characterization of thermo-sensitive hydrogels based on poly(N-isopropylacrylamide)/hyaluronic acid. *Polymer Bulletin*, *67*, 101-124.
- Cornette, V., Ramirez-Pastor, A.J., & Nieto, F. (2003). Percolation of polyatomic species on a square lattice. *The European Physical Journal B*, *36*, 391-399.
- Delbarre-Ladrat, C., Siquin, C., Lebellenger, L., Zykwinska, A., & Colliec-Jouault, S. (2014). Exopolysaccharides produced by marine bacteria and their applications as glycosaminoglycan-

like molecules. *Frontiers in Chemistry*, 2, 85.

Deshmukh, S. A., Sankaranarayanan, S. K. R. S., Suthar, K., & Mancini, D. C. (2012). Role of solvation dynamics and local ordering of water in inducing conformational transitions in poly(N-isopropylacrylamide) oligomers through the LCST. *The Journal of Physical Chemistry. B*, 116, 2651-2663.

D'Este, M., Sprecher, C. M., Milz, S., Nehrbass, D., Dresing, I., Zeiter, S., Alini, M., & Eglin, D. (2016). Evaluation of an injectable thermoresponsive hyaluronic acid hydrogel in a rabbit osteochondral defect model. *Journal of Biomedical Materials Research*, 104, 1469-1478.

Ding, H., Li, B., Liu, Z., Liu, G., Pu, S., Feng, Y., Jia, D., & Zhou, Y. (2020). Decoupled pH- and thermo-responsive injectable chitosan/PNIPAM hydrogel via thiol-ene click chemistry for potential applications in tissue engineering. *Advanced Healthcare Materials*, 9, 2000454.

Essmann, U., Perera, L., Berkowitz, M. J., Darden, T., Lee, H., & Pedersen, L. G. (1995). A smooth particle mesh Ewald method. *The Journal of Chemical Physics*, 103, 8577-8593.

Fuentes, C., Choi, J., Zielke, C., Peñarrubia, J. M., Lee, S., & Nilsson, L. (2019). Comparison between conventional and frit-inlet channels in separation of biopolymers by asymmetric flow field-flow fractionation. *Analytica Chimica Acta*, 144, 4559-4568.

Fujishige, S., Kubota, K., & Ando, I. (1989). Phase transition of aqueous solutions of poly(N-isopropylacrylamide) and poly(N-isopropylmethacrylamide). *The Journal of Physical Chemistry*, 93, 3311-3313.

Gandhi, N. S. & Mancera, R. L. (2008). The structure of glycosaminoglycans and their interactions with proteins. *Chemical Biology & Drug Design*, 72, 455-482.

Gélébart, P., Cuenot, S., Siquin, C., Halgand, B., Sourice, S., Le Visage, C., Guicheux, J., Collic-Jouault, S., & Zykowska, A. (2022). Microgels based on Infernan, a

glycosaminoglycan-mimetic bacterial exopolysaccharide, as BMP-2 delivery systems. *Carbohydrate Polymers*, 284, 119191.

Guo, H., Brûlet, A., Rajamohanam, P. R., Marcellan, A., Sanson, N., & Hourdet, D. (2015). Influence of topology of LCST-based graft copolymers on responsive assembling in aqueous media. *Polymer*, 60, 164-175.

Guo, H., de Magalhaes Goncalves, M., Ducouret, G., & Hourdet, D. (2018). Cold and hot gelling of alginate-graft-PNIPAM: a schizophrenic behavior induced by potassium salts. *Biomacromolecules*, 19, 576-587.

Humphrey, W., Dalke, A., & Schulten, K. (1996). VMD - Visual Molecular Dynamics. *Journal of Molecular Graphics*, 14, 33-38.

Kang, Z., Zhou, Z., Wang, Y., Huang, H., Du, C. & Chen, J. (2018). Bio-based strategies for producing glycosaminoglycans and their oligosaccharides. *Trends in Biotechnology*, 36, 806-818.

Kirschner, K. N., Yongye, A. B., Tschampel, S. M., Gonzalez-Outeirino, J., Daniels, C. R., Foley, B. L., et al. (2008). GLYCAM06: A generalizable biomolecular force field. Carbohydrates. *Journal of Computational Chemistry*, 29, 622-655.

Lee, H., Kim, J. Y., Choi, W., & Moon, M. H. (2017). Effect of cationic monomer content on polyacrylamide copolymers by frit-inlet asymmetrical flow field-flow fractionation/multi-angle light scattering. *Journal of Chromatography. A*, 1503, 49-56.

Lima, L. R. M., Cavalcante, C. M. W. S. A., Carneiro, M. J. M., Mendes, J. F. S., Sousa, N. A., Freire, R. S., Pinto, V. P. T., Fontenelle, R. O. S., Feitosa, J. P. A., & de Paula, R. C. M. (2021). Thermal responsive poly-N-isopropylacrylamide/galactomannan copolymer nanoparticles as a potential amphotericin delivery carrier. *Carbohydrate Polymer Technologies and Applications*,

2, 100126.

Liu, K., Guo, L., Chen, X., Liu, L., & Gao, C. (2023). Microbial synthesis of glycosaminoglycans and their oligosaccharides. *Trends in Microbiology*, *31*, 369-383.

Makshakova, O., Zykwincka, A., Cuenot, S., Collic-Jouault, S., & Perez, S. (2022). Three-dimensional structures, dynamics and calcium-mediated interactions of the exopolysaccharide, Infernan, produced by the deep-sea hydrothermal bacterium *Alteromonas infernus*. *Carbohydrate Polymers*, *276*, 118732.

Menezes, R., Vincent, R., Osorno, L., Hu, P., & Arinzeh, T. I. (2023). Biomaterials and tissue engineering approaches using glycosaminoglycans for tissue repair: lessons learned from the native extracellular matrix. *Acta Biomaterialia*, *163*, 219-227.

Mortisen, D., Peroglio, M., Alini, M., & Eglin, D. (2020). Tailoring thermoreversible hyaluronan hydrogels by “click” chemistry and RAFT polymerization for cell and drug therapy. *Biomacromolecules*, *11*, 1261-1272.

Ono, Y., & Shikata, T. (2006). Hydration and Dynamic Behavior of Poly(N-isopropylacrylamide)s in Aqueous Solution: A Sharp Phase Transition at the Lower Critical Solution Temperature. *Journal of the American Chemical Society*, *128*, 10030-10031.

Ortiz de Solorzano, I., Pejagam, K. K., An, Y., Singh, S. K., & Deshmukh, S. A. (2020). Solvation dynamics of N-substituted acrylamide polymers and the importance for phase transition behavior. *Soft Matter*, *16*, 1582-1593.

Petit, L., Karakasyan, C., Pantoustier, N., & Hourdet, D. (2007). Synthesis of graft polyacrylamide with responsive self-assembling properties in aqueous media. *Polymer*, *48*, 7098-7112.

Perez, S., Makshakova, O., Angulo, J., Bedini, E., Bisio, A., de Paz, J. L., Fadda, E., Guerrini,

M., Hricovini, M., Hricovini, M., Lisacek, F., Nieto, P. M., Pagel, K., Paiardi, G., Richter, R., Samsonov, S. A., Vivès, R. R., Nikitovic, D., & Ricard Blum, S. (2023). Glycosaminoglycans: what remains to be deciphered? *Journal of American Chemical Society*, *3*, 628-656.

Raguénès, G. H. C., Peres, A., Ruimy, R., Pignet, P., Christen, R., Loaec, M., Rougeaux, H., Barbier, G., & Guezennec, J. G. (1997). *Alteromonas infernus* sp. Nov., a new polysaccharide-producing bacterium isolated from a deep-sea hydrothermal vent. *Journal of Applied Microbiology*, *82*, 422-430.

Rana, M. M., & De la Hoz Siegler, H. (2021). Tuning the properties of PNIPAm-based hydrogel scaffolds for cartilage tissue engineering. *Polymers*, *13*, 3154.

Rederstorff, E., Rethore, G., Weiss, P., Sourice, S., Becq-Cormier, S., Mathieu, E., Maillasson, M., Jacques, Y., Collic-Jouault, S., Fellah, B. H., Guicheux, J., & Vinatier, C. (2017). Enriching a cellulose hydrogel with a biologically active marine exopolysaccharide for cell-based cartilage engineering: Polysaccharide hydrogel for cartilage engineering. *Journal of Tissue Engineering and Regenerative Medicine*, *11*, 1152-1164.

Rederstorff, E., Weiss, P., Sourice, S., Pilet, P., Xie, F., Siquin, C., Collic-Jouault, S., Guicheux, J., & Läub, S. (2011). An *in vitro* study of two GAG-like marine polysaccharides incorporated into injectable hydrogels for bone and cartilage tissue engineering. *Acta Biomaterialia*, *7*, 2119-2130.

Roger, O., Kervarec, N., Ratiskol, J., Collic-Jouault, S., & Chevolut, L. (2004). Structural studies of the main exopolysaccharide produced by the deep-sea bacterium *Alteromonas infernus*. *Carbohydrate Research*, *339*, 2371-2380.

Ruel-Gariépy, E., & Leroux, J.-C. (2004). In situ-forming hydrogels - review of temperature-sensitive systems. *European Journal of Pharmaceutics and Biopharmaceutics*, *58*, 409-426.

Ryckaert, J. P., Ciccotti, G., & Berendsen, H. J. C. (1997). Numerical integration of the Cartesian equations of motion of a system with constraints; molecular dynamics of n-alkanes. *Journal of Computational Physics*, *23*, 327–341.

Safakas, K., Saravanou, S.-F., Iatridi, Z., & Tsitsilianis, C. (2021). Alginate-g-PNIPAM-based thermo/shear-responsive injectable hydrogels: tailoring the rheological properties by adjusting the LCST of the grafting chains. *International Journal of Molecular Sciences*, *22*, 8.

Shin, D. Y., Hwang, E., Cho, I.-H., & Moon, M. H. (2007). Molecular weight and structure characterization of sodium hyaluronate and its gamma radiation degradation products by flow field-flow fractionation and on-line multiangle light scattering. *Journal of Chromatography A*, *1160*, 270-275.

Tavagnacco, L., Zaccarelli, E., & Chiessi, E. (2010). On the molecular origin of the cooperative coil-to-globule transition of poly(N-isopropylacrylamide) in water. *Physical Chemistry Chemical Physics*, *20*, 9997-10010.

ter Boo, G.-J. A., Richards, R. G., Moriarty, T. F., Grijpma, D. W., & Eglin, D. (2017). Hyaluronic acid derivatives and its polyelectrolyte complexes with gentamicin as a delivery system for antibiotics. *Polymer for Advanced Technologies*, *28*, 1325-1333.

Tzounis, P.-N., Anogiannakis, S.D., & Theodorou, D.N. (2017). General Methodology for estimating the stiffness of polymer chains from their chemical constitution: a single unperturbed chain Monte Carlo algorithm. *Macromolecules*, *50*, 4575-4587.

Vasile, C., & Nita, L. E. (2011). Novel multi-stimuli responsive sodium alginate-grafted-poly(N-isopropylacrylamide) copolymers: II. Dilute solution properties. *Carbohydrate Polymers*, *86*, 77-84.

Wang, J., Wolf, R. M., Caldwell, J. W., Kollman, P. A., & Case, D. A. (2004). Development and

testing of a general AMBER force field. *Journal of Computational Chemistry*, 25, 1157-1174.

Wang, J., Wang, W., Kollman P. A., & Case, D. A. (2006). Automatic atom type and bond type perception in molecular mechanical calculations. *Journal of Molecular Graphics and Modelling*, 25, 247260.

Wu, Y., Schmittmann, B., & Zia, R.K.P. (2008). Two-dimensional polymer networks near percolation. *Journal of Physics A: Mathematical and Theoretical*, 41, 025004.

Yan, Y., Huang, L., Zhang, Q., & Zhou, H. (2015). Concentration effect on aggregation and dissolution behavior of poly(*N*-isopropylacrylamide) in water. *Journal of Applied Polymer Science*, 132, 41669.

Zykwinska, A., Marchand, L., Bonnetot, S., Siquin, C., Collic-Jouault, S., & Delbarre-Ladrat, C. (2019a). Deep-sea hydrothermal vent bacteria as a source of glycosaminoglycan-mimetic exopolysaccharides. *Molecules*, 24, 1703.

Zykwinska, A., Marquis, M., Godin, M., Marchand, L., Siquin, C., Garnier, C., Jonchère, C., Chédeville, C., Le Visage, C., Guicheux, J., Collic-Jouault, S., & Cuenot, S. (2019b). Microcarriers based on glycosaminoglycan-like marine exopolysaccharide for TGF- β 1 long-term protection. *Marine Drugs*, 17, 55.

Zykwinska, A., Maksharova, O., Gélébart, P., Siquin, C., Stephant, N., Collic-Jouault, S., Perez, S., & Cuenot, S. Interactions between infernan and calcium: from the molecular level to the mechanical properties of microgels. (2022). *Carbohydrate Polymers*, 292, 119629.

Zykwinska, A., Pihet, M., Radji, S., Bouchara, J-P., & Cuenot, S. (2014). Self-assembly of proteins into a three-dimensional multilayer system: investigation of the surface of the human fungal pathogen *Aspergillus fumigatus*. *Biochimica Biophysica Acta*, 1844, 1137-1144.

Declaration of interests

The authors declare that they have no known competing financial interests or personal relationships that could have appeared to influence the work reported in this paper.

The authors declare the following financial interests/personal relationships which may be considered as potential competing interests: